REPORT DOCUMENTATION PAGE

The public reporting burden for this collection of information is estimated to average 1 hour per response, including the time for reviewing instructions, searching existing data sources, gathering and maintaining the data needed, and completing and reviewing the collection of information. Send comments regarding this burden estimate or any other aspect of this collection of information, including suggestions for reducing the burden, to Department of Defense, Washington Headquarters Services, Directorate for Information Operations and Reports (0704-0188), 1215 Jefferson Davis Highway, Suite 1204, Arlington, VA 22202-4302. Respondents should be aware that notwithstanding any other provision of law, no person shall be subject to any penalty for failing to comply with a collection of information if it does not display a currently valid OMB control number.
PLEASE DO NOT RETURN YOUR FORM TO THE ABOVE ADDRESS.

1. REPORT DATE (DD-MM-YYYY)	2. REPORT TYPE		3. DATES COVERED (From - To)
28June2007	Final Report		1March2002-30September2006

4. TITLE AND SUBTITLE	5a. CONTRACT NUMBER
Detonation Initiation and Evolution in Spray-Fueled Pulsed Detonation Rocket Engines	
	5b. GRANT NUMBER
	F49620-02-1- 0121
	5c. PROGRAM ELEMENT NUMBER

6. AUTHOR(S)	5d. PROJECT NUMBER
David R. Kassoy	
	5e. TASK NUMBER
	5f. WORK UNIT NUMBER

7. PERFORMING ORGANIZATION NAME(S) AND ADDRESS(ES)	8. PERFORMING ORGANIZATION REPORT NUMBER
University of Colorado, Mechanical Engineering, 427 UCB Boulder Colorado, 80309-0427	

9. SPONSORING/MONITORING AGENCY NAME(S) AND ADDRESS(ES)	10. SPONSOR/MONITOR'S ACRONYM(S)
AFOSR/NA 801 N. Randolph St. Rm. 732 Arlington VA 22203 Dr Mitat Birkan	
	11. SPONSOR/MONITOR'S REPORT NUMBER(S)

12. DISTRIBUTION/AVAILABILITY STATEMENT
Unlimited, Approved for public release

AFRL-SR-AR-TR-07-0225

13. SUPPLEMENTARY NOTES

14. ABSTRACT

Successful pulsed detonation engine operation requires robust, reliable, repetitive detonation initiation and evolution, up to 100 times per second. Spark-initiated combustion of fuel-oxidizer mixtures appears to be the operational technology. Our research program was designed to model the transient events following time-resolved deposition of thermal energy into a finite volume of reactive mixture. Computational solutions of the reactive Euler equations are used to predict the time history of deflagration to detonation transitions (DDT's). Solutions describe the temporal variation of the spatial distributions of temperature, pressure and fuel concentration.. The presence of shocks, localized reactive hot spots and high speed reaction zones are noted. Solution dependence on the location of the initial power deposition, the amount of power deposition and the activation energy on a one step reaction is investigated. In all cases the DDT process is facilitated by the spontaneous appearance of localized high pressure and temperature ":reaction centers" that are the subsequent sources of acoustic compression waves.

15. SUBJECT TERMS

reactive gasdynamics, detonation initiation, deflagration-to-detonation transition

16. SECURITY CLASSIFICATION OF:			17. LIMITATION OF ABSTRACT	18. NUMBER OF PAGES	19a. NAME OF RESPONSIBLE PERSON
a. REPORT	b. ABSTRACT	c. THIS PAGE			David R. Kassoy
U	U	U	UU	85	19b. TELEPHONE NUMBER (Include area code) 303 4926066

Detonation Initiation and Evolution in Spray-Fueled Pulsed Detonation Rocket Engines

Grant No. F49620-02-1-0121

Final Report Period

1March2002-30September2006

prepared for

Dr. Mitat Birkan
AFOSR/NA
801 N. Randolph St., Rm. 732
Arlington, VA 22203

D. R. Kassoy, Professor
Department of Mechanical Engineering
University of Colorado, Boulder
Boulder, CO. 80309-0427

June 28, 2007

Table of Contents

Detonation initiation on the microsecond time scale: DDTs

D. R. KASSOY[†], J. A. KUEHN[‡], M.W. NABITY[*], J. F. CLARKE[§]

Spatially resolved, thermal power deposition of limited duration into a finite volume of reactive gas is the initiator for a deflagration-to-detonation transition (DDT) on the microsecond time scale. The reactive Euler equations with one-step Arrhenius kinetics are used to derive novel formulas for velocity and temperature variation that describe the physical phenomena characteristic of DDTs. A transformation of the variables is shown to yield a canonical equation system, independent of the activation energy. Numerical solutions of the reactive Euler equations are used to describe the detailed sequence of reactive gasdynamic processes leading to an overdriven planar detonation far from the power deposition location. Results are presented for deposition into a region isolated from the planar boundary of the reactive gas as well as for that adjacent to the boundary. The role of compressions and shocks reflected from the boundary into the partially reacted hot gas is described. The quantitative dependences of DDT evolution on the magnitude of thermal power deposition and activation energy are identified.

Keywords: reactive gasdynamics, detonation initiation, deflagration-to-detonation transition

[†] Professor, Mechanical Engineering, University of Colorado, 427 UCB, Boulder, CO 80309
[‡] Computer Science and Mathematics Division, Oak Ridge National Laboratory, One Bethel Valley Road MS-6173, Oak Ridge, TN 37831
[*] Graduate Student, Applied Mathematics, University of Colorado, 526 UCB, Boulder, CO 80309
[§] Professor Emeritus, Cranfield University, Cranfield, UK

1 Introduction

"Gasdynamics of explosions is...best defined as the science dealing with the interrelationship between energy transfer occurring at a high rate in a compressible medium and the concomitant motion set up in the this medium" (Oppenheim and Soloukhin, 1973). The dynamics of the interaction depend on the relationship between the dimensional time scale for substantial chemical heat release, t'_H, into a local region of length scale ℓ', and local acoustic time $t'_A = \ell'/a'$ where a' is the local speed of sound. When $t'_H \ll t'_A$ local heat addition occurs in a basically constant volume process (local inertial confinement) because the fluid cannot respond on the short time scale (Kassoy and Palaniswamy, 2002). The temperature rise is accompanied by a concomitant pressure rise, so that for a brief instant a high-pressure spot exists in a relatively low pressure and temperature environment. Subsequent expansion of the spot on the local t'_A-time scale, driven by the large pressure gradient between the spot and the environment is the source ("piston" effect) of compression waves in the environment. Wave coalescence can lead to shock wave formation. Partial inertial confinement occurs in the less exteme case $t'_H = O(t'_A)$ so that localized pressure increase with heat release is still possible although the expansion process occurs simultaneously with the heat addition, limiting the pressure rise and the amplitude of the compression waves. "Concomitant to (these ideas) is the appreciation of the role played in the detonation process by the power density....at which energy is deposited into the compressible medium" (Oppenheim and Soloukhin, 1973). This quote refers to reactive gasdynamic **transients** specifically, where gasdynamic wave generation following a high rate of localized heat addition is

2

crucial to facilitating fast, high temperature reaction rates. In contrast, the chemical heat release rate is insignificant for a steadily propagating Chapman-Jouguet (C.J.) wave (Fickett and Davis, 1979).

The evolutionary process of detonation formation following thermal power deposition into a reactive mixture is fundamentally dependent on reactive gasdynamic transients. Experiments of this type in a tube (Oppenheim,1985) begin with a laminar flame initiated by a spark. A myriad of instabilities cause the flame to become wrinkled (Khokhlov, Oran, and Thomas,1999, and Khokhlov and Oran, 1999), thus enhancing the rate of energy production through area enhancement. The resulting turbulent flame brush is observed to be the source of gasdynamic compression waves propagating forward into the initially undisturbed reactive mixture. The local reaction rate is enhanced by temperature increases caused by compression wave passage. Eventually a definitive localized "explosion in an explosion" occurring on the tube boundary is the source of strong shocks which coalesce with previously generated compression waves to form a shock capable of inducing substantial chemical heat release immediately downstream of the wave front. It is possible that a transient ZND detonation wave is produced first. However, in experiments all such waves evolve to a three dimensional cellular structure, Lee,(1984). A very considerable literature describes experimental and modeling studies of one and two dimensional instabilities of initially planar ZND-waves.(see, for example, Gamezo, Desbordes and Oran, 1999, Sharpe and Falle, 1999, 2001, Sharpe,2001, Kasimov and Stewart, 2004 for reviews of major contributions). The emphasis is on highly accurate algorithms, capable of resolving the evoution of a steady C.J. wave to

either one dimensional transient dynamics predicted by linear stability theory(Lee and Stewart, 1990, Sharpe, 1997, Stewart and Kasimov, 2006) and to two dimensional transient dynamics, including triple points and other transverse wave phenomena. Stability-related modeling is distinct from that describing the appearance of planar or two dimensional detonations following a defined localized thermal disturbance, of interest for facilitating robust, reliable, repetitive detonation initiations in a pulsed detonation engine. (Schauer, Miser, Tucker, Bradley and Hoke, 2005).

Dold et al. (1995) have used an initial-boundary value solution approach for the Euler equations to find one-dimensional detonations arising from an initially imposed, spatially distributed pressure pulse. Although thermal initiation is absent, the imposed pressure disturbance steepens into shocks that create the high temperature regimes necessary for rapid acceleration of reaction rates and the appearance of multiple ignition sites. The sequence of events leading to detonation formation are more than reminiscent of the events in thermal initiation models by Clarke, Kassoy, and Riley (1986) and Clarke, Kassoy, Meharzi, Riley, and Vasantha (1990), and Sileem, Kassoy, and Hayashi (1991) (SKH). This qualitative agreement, with in fact quite similar time scales of transition to detonation for similar activation energy values, is very encouraging because the numerical method employed is unlike the MacCormack scheme used in SKH.

Sileem, Kassoy and Hayashi (1991)(SKH) model the evolution of planar detonation formation following time and spatially resolved thermal power into a finite volume of reactive gas. The reactive Euler equations with one-step Arrhenius kinetics, scaled so that $t'_A = O(t'_A)$ are solved numerically. The evolution to detonation is described in terms

4

of a sequence of localized chemical heat addition events leading to gasdynamic wave generation and strong shock formation, reminiscent of Oppenheim's(1985) observations. An overdriven ZND-detonation is born initially, similar to the experimental observations of Moen, Donato, Knystautas and Lee (1980) and Schauer et. al. (2005), in the context of an evolving turbulent flame. The transient ZND wave relaxes spontaneously to a stable CJ wave appropriate to the mixture parameters. These results demonstrate that, from a mathematical perspective, transverse waves and turbulence are not essential for detonation formation. A physically reasonable sequence of planar reactive gasdynamic processes featuring accelerating localized chemical power deposition, concomitant pressure increases and subsequent compression wave generation, is sufficient to ensure the outcome.

Smirnov and Panfilov (1995) describe planar deflagration to detonation transition in a chemically reactive, viscous, conductive gas with a two step kinetic model. Thermal initiators included boundary heating, like that in Clarke et al. (1986, 1990) and a pre-existing localized high temperature spot. A pre-existing, small, localized temperature gradient is used by Kapila et al. (2002) to initiate a planar detonation, as first suggested by Zeldovich (1970, 1980). Euler equations and a one-step kinetic model are used. The Kapila et al. paper includes an extensive literature survey of related work for both deflagration-to detonation (DDT) processes and direct initiation. More recently, Gu et al. (2003) have modeled the formation of spherical detonations arising from a pre-existing localized hot spot on the millimeter length scale. The initial spot temperature distribution is characterized by a linear temperature gradient with a maximum temperature only very

slightly higher than that of the surrounding environment. The chemically reactive, viscous, conductive gas equations are used along with a hydrogen-oxygen kinetic scheme. Chemical heat release occurs on a microsecond time scale. The evolutionary process to detonation is found to be quite sensitive to the characteristic initial gradient present.

The two-dimensional reactive Navier-Stokes equations with one step kinetics are used by Tegner and Sjögreen to model transitions from deflagration to detonation arising from a suddenly imposed hot spot. An "accelerating (laminar) flame" is the initial source of a lead shock wave which "preconditions" the unburned mixture. The aforementioned reactive gasdynamics processes follow.

Sharpe and Falle (1999) describe one-dimensional evolution of an initially CJ wave, based on solutions to the Euler equations with one step chemistry. Numerical noise provides the disturbances that yield planar transient responses reminiscent of those seen in the SKH initiation study, including the appearance of unburned pockets of reactive mixture well behind the gasdynamic wave front. The irregularity of the transients, defined by the time history of the post shock pressure, is strongly dependent on the activation energy. These one-dimensional simulations require significant reaction zone resolution.

Kasimov and Stewart (2004) use a novel numerical algorithm for integration of the reactive one-dimensional Euler equations with one step kinetics in a shock-attached frame, to describe "....the dynamics of self-sustained detonation waves...." Conditions on the upstream boundary are given careful attention to minimize the impact of spurious

reflected gasdyamic waves on the interior solution. Solution accuracy requires several hundred grid points per half-reaction length. Higher activation energy mixtures exhibit irregular reactive gasdynamics. So called "re-ignition" events are characterized by the appearance of localized high pressure spots, shown in Fig. 9, which are correlated with locally high rates of chemical heat release.

Pre-existing strong blast waves can be employed to create detonations in a more immediate way than is typical in a DDT. Mazaheri (1997) and Eckett et al. (2000) have modeled direct initiation of planar and spherical detonations, respectively, following the instantaneous appearance of a blast wave. The modeling is based on one-step kinetics. These studies predict critical energies required for self-sustained detonations as well as evolution scenarios for failing detonations.

There is an extensive related literature describing initial-boundary value solutions to the Euler equations for mechanically driven plane detonations. Typically, a piston motion is prescribed in order to propagate a relatively strong shock into the reactive gas. Singh and Clarke (1991) provide a review of the subject, as well as numerical solutions found by using a random choice method.

Related efforts in computational modeling of two-dimensional initiation of, and transition to detonation, are described by Nikiforakis and Clarke (1996). A computational solution is obtained to an initial-boundary value problem described by the reactive Euler equations. The initiator in this case is a planar reflected shock propagating through a spot with an imposed, slightly elevated temperature located adjacent to the closed endwall of a shock tube in an asymmetric position. The relatively high, spatially non-uniform

temperature behind the reflected shock accelerates the local reactions and thereby initiates the desired transient reactive gasdynamic events. These planar studies predict wave patterns like those seen in the observations of Meyer and Oppenheim (1971).

Gamezo et.al. (1999) use the Euler equations with one step chemistry to model the evolution of an initially overdriven planar detonation subjected to numerical noise. After a period of attenuation toward a steady, planar CJ wave, two-dimensional perturbations of the shock front and reaction zone begin to appear. The detonation front evolves to an unsteady ensemble of transverse waves and triple-shock configurations propagating at an average axial speed of a planar CJ speed. The regularity of the cell structure and the transient characteristics of the transverse phenomena on the wave front are quite sensitive to the activation energy.

Strong transverse wave evolution from a disturbed planar CJ wave is also considered by Sharpe (2001). The two dimensional reactive Euler equations with a one step kinetics model are solved numerically. A spatially resolved density inhomogeneity is used to disturb the initially planar wave. High resolution simulations are used to examine the two dimensional structure of the wave front, including collisions of the triple points propagating transversely, and transverse phenomena just behind the front.

The primary objective of the current modeling study is to extend the SKH study to a broader range of parameters, including the initiating thermal power deposition, the location of the power deposition and the activation energy, to identify "...the interrelationship between energy transfer occurring at a high rate in a compressible medium and the concomitant motion set up in the this medium". Although this initial

value study is limited to one-dimension it provides useful insights into the impact of localized chemical power deposition levels on induced gasdynamic processes.

The late time solutions described in SKH are reexamined to ascertain the source of relatively small solution oscillations that appear as the overdriven detonation, relaxes to the appropriate stable C.J. state. Optimization of the Courant number value and the grid size used in the MacCormack method are used to demonstrate that the oscillation amplitude can be reduced by decreasing the mesh size. These results imply that the oscillation has a numerical origin and can be made as small as desired by grid size reduction. For sufficiently small grid size, the oscillations in several sensitive variables are nearly negligible.

Prior to the computational study, the describing equations are used as the basis for a qualitative discussion of the physicochemical processes occurring in the system. A novel description is given of the relationship between localized thermal power deposition in the gas, the appearance of confined high pressure and temperature regions, the impact of shock waves evolving in a reactive atmosphere, and the gas velocity field induced by the energetics (Kassoy, Kuehn, Nabity, and Clarke, 2005). It is also shown that a transformation of the variables can remove the activation energy from the Euler equations. The canonical equations are cited in Eulerian and Lagrangian form. Further analysis will appear in a future paper.

Finally, computational results are used to quantify the impact of thermal power deposition location and amplitude as well as activation energy on the evolution of detonation formation. In effect, one-dimensional models are usually based on a

symmetric initiating disturbance relative to the geometrical configuration of the spatial region. The current work features spatially distributed heating on the microsecond time scale into a localized region at a finite distance from a confining planar boundary (wall). The initial burst of thermal power into the asymmetrically located target volume causes a significant local temperature and pressure rise. As a result, strong compressive gasdynamic waves propagate both upstream and downstream. The upstream waves reflect from the wall and evolve into strong shocks propagating through previously compressed, partially burned gas mixture. The wave reflections alter the overall process of detonation formation relative to that found with symmetric power deposition.

2 Formulation

The nondimensional mathematical model for a compressible gas with a one step exothermic Arrhenius reaction, derived by SKH for a wide range of physical and chemical conditions as well as length and time scales can be written in the form:

$$p = \rho T \tag{1}$$

$$\rho_s + (\rho u)_z = 0 \quad , \tag{2}$$

$$\rho(u_s + u u_z) = -p_z/\gamma \quad , \tag{3}$$

$$(\rho C_v/(\gamma-1))(T_s + u T_z) = -pu_z + \rho \hat{Q} + (\rho \hat{B} q Y/(\gamma-1))\exp(-1/\varepsilon^* T) \quad , \tag{4}$$

$$Y_s + u Y_z = -(\hat{B} Y/\gamma)\exp(-1/\varepsilon^* T) \quad , \tag{5}$$

The thermodynamic variables (p, ρ, T) are nondimensionalized with respect to an undisturbed initial state (p_o', ρ_o', T_o') and the speed u with the undisturbed speed of sound

a'_o, where $a'^2_o = \gamma R' T'_o$. Also, the inverse activation energy parameter ε^* is defined with respect to T'_o.

The nondimensional thermal power source per unit mass $\hat{Q}$ is absorbed on a dimensional length scale characterized by ℓ' with a duration characterized by the acoustic time of the heated domain $t'_A = \ell'/a'_o \left(t'_H = O(t'_A) \right)$. It follows that

$$\hat{Q} = [\gamma/(\gamma-1)][\ell'/a'_o][Q'/C'_{po}T'_o] \quad , \quad \hat{B} = \gamma \ell' B'/a'_o \quad \gamma = C'_{po}/C'_{vo} \qquad (6)$$

where B' is the preexponential factor in the Arrenhius rate law. Further, the space and time variables are nondimensionlized by using ℓ' and ℓ'/a'_o, respectively. The nondimensional heat of reaction, $q = q'/C'_{po}T'_0$, where q' is the dimensional value. The remaining variables are defined in standard ways.

Relative to the terms shown in Equations (3)-(5), SKH also show that transport terms are proportional to the Knudsen number $\mu'_o/\rho'_o\ell'a'_o$ which is typically very small. In general, the Euler-forms of the equations are valid when ℓ' is significantly larger than the molecular mean free path and far smaller than the axial length of a laboratory detonation tube. The latter condition ensures that a wave process initiated near the left-hand wall will not reach a right hand boundary for s-values of interest. Further, the equations describe the time history of a spatially varying process everywhere, except in shocks which are described by jump conditions across a discontinuity.

Initially, the undisturbed system is described by

$$s = 0 \quad , \quad p = \rho = T = Y = 1, u = 0 \quad , \quad z > 0 \quad . \qquad (7)$$

Conditions at the impermeable left hand boundary are described by

$$z = 0 \quad , \quad u = Y_z = T_z = 0 \quad . \tag{8}$$

The entire reactive event is initiated at $s = 0^+$ by depositing a finite amount of power $\hat{Q}$ for a specific period of time into a localized asymmetric region adjacent to, or near the left hand boundary, defined in this work by:

$$\rho \hat{Q} = 0 \quad , \qquad\qquad\qquad 0 \leq z \leq z_i - 2 \tag{9}$$

$$= 3\gamma f(s) \cos\left[\frac{\pi}{4}[z_i - z]\right] \quad (z_i - 2) < z \leq (z_i + 2) \tag{10}$$

$$= 0 \qquad\qquad\qquad z > z_i + 2 \tag{11}$$

where $z_i = 2$, 3 or 4 and

$$f(s) = 0.7\left[\tanh \ 5\left(s - \tfrac{1}{2}\right) - \tanh 5(s - 10)\right] \tag{12}$$

In effect the initiating power deposition terminates very close to the switch off time $s = 10$. It is noted that the spatial structure in (9)-(11) differs from that employed by SKH.

The wave system evolving from the initiating power deposition process propagates into a relatively cold gas with a characteristic spatially homogeneous thermal explosion time $s_e = \varepsilon^* e^{1/\varepsilon^*} / \hat{B}q$, which is typically significantly larger than the time scale required for a C.J. detonation to evolve from the initiating event (e.g., $s = O(10)$). For example, the parameters used in SKH ($\varepsilon^* = 0.08$, $\hat{B} = 15$, $q = 6$) give $s_e = 238.5$. It follows that the change in T in front of the oncoming wave system will be very small (perhaps 1%) compared to that in the system for s-values of interest. Nonetheless, it is useful to allow the slow, spatially homogeneous reaction ahead of the wave system to occur in order to

12

carry out the smoothest possible initial value calculation. In effect, the lead shock propagates into a slightly depleted (perhaps 1%) reactive mixture.

3 Properties of the Describing Equations

A qualitative understanding of the physical processes occurring in a transient compressible flow with localized heat addition from exothermic reactions can be obtained from the mathematical properties of Equations (1)-(5). In particular, it is useful to demonstrate the relationship between thermal power deposition into the gas and the resulting induced gasdynamic processes, including the appearance and evolution of shock waves.

Equations (1), (2), and (4) can be combined [Kassoy et al. 2005] to show that

$$u_z = \frac{(\gamma-1)}{\gamma}\frac{\hat{Q}}{C_pT} + \frac{\hat{B}qY}{\gamma C_pT}e^{-1/\varepsilon'T} - \frac{C_v}{\gamma C_p p}\frac{Dp}{Ds} \quad , \tag{13}$$

in any flow region where the derivatives are defined (e.g., not including shock discontinuities). Here $D/Ds = (\partial/\partial s + u\partial/\partial z)$. At a given time value s, one may integrate Equation (13) continuously from a left hand boundary (which may be just to the right of a shock wave) to any larger value z prior to the location of the next shock downstream. If, in addition, one accounts for the velocity jumps $(\Delta u)_i = u_i^+ - u_i^-$ across each of n shock discontinuities located at z_{si};

$$u(z,s) = \int_0^z \left[\frac{\gamma-1}{\gamma}\frac{\hat{Q}}{C_pT} + \frac{\hat{B}qY}{\gamma C_pT}e^{-1/\varepsilon'T} - \frac{C_v}{\gamma C_p p}\frac{Dp}{Ds} \right]d\bar{z} + \sum_{i=1}^n (\Delta u)_i \quad , \tag{14}$$

where the integral is written for piecewise continuous functions in each interval $z_{si} < z < z_{s(i+1)}$, and the first of (8) is satisfied. Here $(\Delta u)_i$ may be positive or negative, depending on the difference in velocity just to the right of (+) and just to the left of (−), a shock which may move to the right or left. If the lead shock is located at $z_{s(n+1)}(s)$, then the velocity jump across the shock must be equal to the negative of the induced speed just behind the shock: $(\Delta u)_{n+1} = -u(z^-_{s(n+1)}, s) \equiv -u^-_s$. Here, u^-_s is the "piston speed" supporting the lead shock [Liepman and Roshko 1984b].

Equation (14) can be used as a diagnostic tool to interpret the role of certain physical effects in the evolving velocity field. The first term in the integrand represents the impact of the initiating power absorption. In general, contributions from this term are limited to finite space and time domains. In the specific case defined in (9)-(12), the spatial integral is nonzero for $(z_i - 2) \le z \le (z_i + 2)$ and $s \le 10$.

The second term in the integrand represents the effect of chemical heat release relative to the enthalpy of the gas. In general, $O(1)$ contributions to this integral are highly localized, existing in regions of significant reactant concentration $(Y > 0)$, and relatively large temperature because ε^* is typically small (although not necessarily in the asymptotic sense of taking a mathematical limit). The amplitude of the temperature dependent function $w = e^{-1/\varepsilon T}/C_p T$ grows relatively rapidly with T for $T < O(1/\varepsilon^*)$ and the relative increase at a given temperature value $w_T/w = O(1/\varepsilon^* T^2)$, but decreases with increasing temperature levels. Table 1 provides values for $w(T)$ when $C_p = 1$ for $1 \le T \le 1/\varepsilon^*$. In hot regions, w is typically 10^{-2} or larger in magnitude. In regions where the

temperature is relatively low, usually prior to passage of a sufficiently strong shock wave, or when the reactant has been expended $Y = 0$ in fully burned regions, the integral of the second term makes little or no contribution. The scaling transformation $\hat{T} = \varepsilon^{\cdot} T$ can be used in the second term to show that then $Y > 0$, the integral makes a sizable contribution if $\hat{B}q\varepsilon^{\cdot} = O(1)$ in the qualitative sense.

Table 1. The values of $w(T)$ for several activation energy parameter and temperature values of interest.

	$w = (1/T)e^{-1/\varepsilon^{\cdot}T}$		
T	$\varepsilon^{\cdot} = .07$	$\varepsilon^{\cdot} = .08$	$\varepsilon^{\cdot} = 0.1$
1	6.25×10^{-7}	3.73×10^{-6}	4.54×10^{-5}
2	3.95×10^{-4}	9.75×10^{-4}	3.37×10^{-3}
3	2.85×10^{-3}	5.17×10^{-3}	1.19×10^{-2}
5	1.15×10^{-3}	1.64×10^{-2}	2.71×10^{-2}
8	2.10×10^{-2}	2.62×10^{-2}	3.85×10^{-2}
$1/\varepsilon^{\cdot}$	2.58×10^{-2}	2.94×10^{-2}	3.68×10^{-2}

Fluid particle compression is described by the last term in the integral. In local regions of partial inertial confinement (nearly constant volume combustion), where the relative compression $(1/p)Dp/Ds$ is important, this term can reduce the rightward induced fluid speed or reverse it. Thus, some thermal power deposition results in an induced flow field, but in regions of near inertial confinement a pressure rise is experienced, and little thermal energy conversion to kinetic energy (the velocity field) takes place. Generally, inertial confinement occurs in regions where the local heat addition time is small compared to the local acoustic time.

The compression term can also be interpreted in a different way by examining the enthalpy form of the energy equation derived from (1), (2), and (4)

$$\frac{C_p}{T}\frac{DT}{Ds} = \frac{(\gamma-1)}{\gamma}\frac{1}{p}\frac{Dp}{Ds} + \frac{(\gamma-1)}{\gamma}\left[\frac{\hat{Q}}{T} + \frac{\hat{B}qY}{(\gamma-1)T}e^{-1/\varepsilon'T}\right] \quad, \tag{15}$$

valid in regions where the derivatives exist. The first term on the right hand side provides compression heating of a fluid particle as a supplement to the other thermal source terms. Equation (15) also provides a measure of the deviation of the fluid particle processes from isentropic conditions that would prevail if the thermal source terms were absent. In addition, one can observe that in spatial domains where $\hat{Q}=0$, where the reactant is burned, $Y=0$ and/or where the temperature is relatively low (see Table 1) the thermal source term is negligible. Each fluid particle behaves isentropically, although the particle entropy will vary from particle to particle, because the physicochemical processes occurring in any particle evolve to the isentropic condition at an entropy level that depends on the detailed time history of the specific particle. Of course, even in the absence of source terms, the entropy of a fluid particle may be altered suddenly, due to the passage of a shock wave.

Equation (13) also implies that fluid particle compression is driven by thermal power deposition in regions of small or zero velocity gradient. In such a region, Equation (2) can be used to show that $D\rho/Ds \approx 0$, implying that a nearly constant volume process is taking place during a brief period of inertial confinement.

Significant localized increases in pressure are one type of gas response to localized chemical power deposition. The appearance of a high pressure domain of finite extent is

followed by a relaxation process in which steep fronted compression waves propagate into the neighboring, usually moving material. Nonlinear processes cause wave steepening and shock formation. Once created, shocks may be located instantaneously at various positions $z_{si}(s)$, mentioned earlier.

The basic describing equations in Equations (1)-(5) can be put into Lagrangian form by using the transformation

$$m(z,s) = \int_0^z \rho d\bar{z} \quad ,$$ (16)

where the integral is taken at a specified time value s in a piecewise manner to account for jumps in density across shock discontinuities. It follows that:

$$p\upsilon = T$$ (17)

$$\upsilon_s = u_m$$ (18)

$$u_s = -p_m$$ (19)

$$\frac{C_v T_s}{(\gamma-1)} = -pu_m + \hat{Q} + \frac{\hat{B}q}{(\gamma-1)} Ye^{-1/\varepsilon\cdot T}$$ (20)

$$Y_s = \frac{-\hat{B}Y}{\gamma} e^{-1/\varepsilon\cdot T}$$ (21)

where $\upsilon = 1/\rho$ is the specific volume. The analogue to (15), for the case of constant specific heats $C_v = C_p = 1$, can be combined with (21) to find

$$T_s = \frac{(\gamma-1)}{\gamma} \upsilon p_s - qYs + \frac{(\gamma-1)}{\gamma} \hat{Q}$$ (22)

In regions unaffected by $\hat{Q}$ (sufficiently large time and/or distance from a thermal power source), one can integrate this expression for a fixed fluid particle (m = constant) from s

= 0. It must be recalled that shocks can intersect the particle at a sequence of times s_i. At those times the derivatives in (22) are undefined, and one must account for jumps in the thermodynamic variables. However, no discontinuity in Y is expected at s_i because the chemical response to a change in state occurs on a finite time scale following shock passage. It follows that

$$T = 1 + q(1-Y) + \frac{(\gamma-1)}{\gamma} \int_0^s v \frac{\partial p}{\partial \hat{s}}\, d\hat{s} + \sum_{i=1}^m \Delta T_i \quad , \quad s_n < s < s_{n+1} \tag{23}$$

where $\Delta T_i = T_i^+ - T_i^-$ and the +/− superscripts refer to locations just ahead of and just behind the shock, respectively. Equation (23) shows that once fuel is fully consumed $Y = 0$ in $s_n < s < s_{n+1}$, the temperature is a superposition of the adiabatic flame value $1 + q$, the accumulated impact of the compression heating time-history described by the integral expression taken in piecewise form, and the net effect of all shocks that have intersected the particle in the past. It is noted that significant net compression heating and/or the passage of strong shocks may raise the particle temperature significantly above the adiabatic value $1 + q$.

The Arrenhius rate law embedded in the energy equation in Equation (20) can be used to define the relative local chemical reaction time

$$s_{CH} = 1 / \hat{B} e^{-1/\epsilon T} \quad , \tag{24}$$

with respect to the duration of the initiating power pulse, $s = O(1)$.

Table 2 gives values of s_{CH} for a small temperature range of interest when $\hat{B} = 15$, the value used in SKH. As long as reasonable amounts of fuel are available, $q = O(1)$ and $C_v = O(1)$, then Equation (20) can be interpreted to mean the substantial changes in the fluid

particle temperature will occur if s_{CH} is not too large. For example, the numbers in Table 2 suggest that during the early phases of the initiating power deposition process, when $\hat{Q} = O(1)$ and $T \approx 1^+$, the gasdynamic phenomena will be essentially inert. However, should a shock wave intersect an initially cold fluid particle and raise its temperature by as little as a factor of two, the value of s_{CH} is reduced drastically for the $\overset{\bullet}{\varepsilon}$ values shown. It follows that the rate of heat addition from chemical processes will increase significantly after shock passage and promote significant increases in fluid particle temperatures. The accelerated chemical heating process is itself enhanced by increasing $\overset{\bullet}{\varepsilon}$.

Table 2. The value of $s_{CH}(T)$ for several activation energy parameter and temperature values of interest.

	$s_{CH} = 1 / \hat{B} e^{-1/\varepsilon \cdot T}$		
T	$\overset{\bullet}{\varepsilon} = 0.07$	$\overset{\bullet}{\varepsilon} = 0.08$	$\overset{\bullet}{\varepsilon} = 0.1$
1	1.07×10^5	1.79×10^4	1.47×10^3
2	84.5	34.53	9.89
3	7.8	4.30	1.87

The chemical kinetics term in (4) can be used to define a nondimensional local (ℓ) heat addition expression,

$$q_{ch\ell}(s,z) = \frac{q'_{ch\ell}}{\left(\gamma p'_o a'_o / \ell'\right)} = \frac{q\hat{B}}{\gamma(\gamma-1)} \rho Y e^{-1/\varepsilon \cdot T} \quad , \tag{25}$$

used to ascertain the instantaneous spatial distribution of the chemical heat release. The global instantaneous heat release is obtained from (25) by integrating from the boundary to the lead shock location $z_{s_{(n+1)}}$ in the piecewise sense,

$$q_{ch}(s) = \frac{q\hat{B}}{\gamma(\gamma-1)} \int_0^{z_{s_{(n+1)}}} \rho Y e^{-1/\dot{\varepsilon}T} dz \quad . \tag{26}$$

Although heat is released in front of the shock location, the magnitude is relatively insignificant because the exponential term is very small, as in Table I. Equations (25) and (26) will be used to interpret the numerical results in Section 6.

4   Scaling transformations

The relative simplicity of (17)-(21) has enabled the discovery of a nonlinear transformation set

$$H = e^{1/\dot{\varepsilon}T} \quad , \quad p = P/\varepsilon^{*1/2} \quad , \quad v = V/\varepsilon^{*1/2} \quad , \quad u = U/\varepsilon^{*1/2} \tag{27}$$

which remove the dependence on $\dot{\varepsilon}$ from (1)-(5) when $q\varepsilon^* = O(1)$ and $\hat{Q}\varepsilon^* = O(1)$. The results are

$$PV \ln H = 1 \tag{28}$$

$$V_s = U_m \tag{29}$$

$$U_s = -P_m \tag{30}$$

$$\frac{C_v}{(\gamma-1)} \frac{H_s}{H(\ln H)^2} = PU_m - (\hat{Q}\varepsilon^*) - \frac{\hat{B}(q\varepsilon^*)}{(\gamma-1)} \frac{1}{H} \tag{31}$$

$$Y_s = -\frac{\hat{B}Y}{\gamma H} \tag{32}$$

20

Finally, the inverse of the Lagrangian transformation in (16) can be written as

$$z = \varepsilon^{*-1/2} \int_0^m V(s,\tilde{m})\,d\tilde{m} \tag{33}$$

The transformation in (27) desensitizes the describing equations (27)-(32) with respect to the value of ε^*. However, it is recognized that the activation energy parameter value plays a role via boundary conditions of the lead shock.

Figure (33) also implies that the length scale transformation,

$$z = X/\varepsilon^{*1/2} \tag{34}$$

can be used with (25) in (1)-(5) to find a primitive variable canonical equation system;

$$P = R/\ln H \tag{35}$$

$$R_s + (RU)_X = 0 \tag{36}$$

$$R(U_s + UU_X) = -P_X/\gamma \tag{37}$$

$$-C_v(H_s + UH_X) = -(\gamma-1)H\ln HU_X + (\gamma-1)H\ln^2 H(\varepsilon^*\hat{Q}) + \ln^2 H\hat{B}(q\varepsilon^*)Y \tag{38}$$

$$Y_s + UY_X = -(\hat{B}Y/\gamma H) \tag{39}$$

where $R = 1/V$ $(\rho = \varepsilon^{*1/2}R)$.

Finally, the global heat addition function in (26) can be transformed to

$$(q_{ch}(s)/q) = (\hat{B}/\gamma(\gamma-1)) \int_0^{X_{s_{n+1}}^{(s)}} (RY/H)\,dX \quad, \tag{40}$$

again independent of ε^*.

Equation (34) implies that a new length scale, associated with the activation energy parameter, can be defined by

$$x' = \left(\ell' / \varepsilon^{\bullet 1/2} \right) X \quad ,$$

suggesting that if the initiating power deposition occurs on the ℓ' – length scale, then the interesting reactive gasdynamics occurs on the scale $\ell' / \varepsilon^{\bullet 1/2}$. Numerical solutions for (28)-(32) and (35)-(39) will be discussed in a future paper to ascertain the significance of the newly discovered transformation in (27).

5   Numerical Method

The numerical solution for (1)-(5) is developed by using a second-order accurate (space and time), explicit finite-difference method of MacCormack (1969), including a flux-corrected transport technique described by Book et al (1975). Considerable detail is provided in SKH and in Sileem (1989).

The CFL-stability criterion must be satisfied at all mesh points. Operationally, the time step must be found from

$$\Delta s = \lambda \Delta z / \left(|u| + a \right) \quad , \tag{41}$$

where λ is the Courant number, Δz is the selected grid size, and a is the local sound speed. Extensive testing has been employed to find optimized values of λ and Δz, as described in Section 6.

As an example, the calculation for $\varepsilon^{\bullet} = 0.08$, $\hat{B} = 15$, $q = 6$, $\gamma = 1.4$, $C_v = C_p = 1$, $Pr = 0.72$, described in SKH for symmetric power addition, has been redone to assess the role of λ and Δz on the time-history of the solution. Particular attention is concentrated on the long-time results for which SKH found oscillatory relaxation of an initially overdriven

22

detonation wave toward an average C.J. state appropriate to the system parameters. After considerable mesh refinement at $\lambda = 0.98$, SKH determined that at $\Delta z = 6.5 \times 10^{-3}$, the amplitudes of oscillations relative to the mean values where typically 6.6% for the postshock pressure, 8.1% for the postshock temperature, and 2.5% for the global heat release $q_{ch}(s)$.

Prior to the appearance of oscillations, the transient reactive gasdynamics appear to be relatively insensitive to grid spacing for $6.5 \times 10^{-3} \le \Delta z \le 5 \times 10^{-2}$. This is not too surprising, given that the most rapid transients occur on a timescale of about five nondimensional units in s *prior* to detonation formation. Thus, reductions in Δz in Equation (26) cause a concomitant decrease in the time step which is already small enough at $\Delta z = 5 \times 10^{-2}$ to resolve the time-history. In contrast, the oscillations after detonation formation occur on a time scale of about 0.25 s units, so that a reduction of Δz by a factor of 10 can radically improve the time resolution.

The SKH study did not definitively identify physical mechanisms as the source of the oscillations. Clearly, numerical processing may have a considerable impact. In particular, the large absolute temperature and pressure values behind the lead shock may promote relatively larger errors in the chemical production term (see (4)) just behind the shock, arising from numerical errors in the temperature itself. This is particularly important for the case of exponential dependence on temperature. For example, a specified error in the temperature, δ, defined by $T = T_E + \delta$, where T_E is the exact

solution, creates an error in the Arrhenius term $F = e^{-1/\varepsilon^* T} = F_E + \Delta F$, where $F_E = e^{-1/\varepsilon^* T_E}$, such that

$$\frac{d\Delta F}{dT_E} = \frac{F_E \delta}{\varepsilon^* T_E^3}\left[\frac{1}{\varepsilon^* T_E} - 2\right] \quad . \tag{42}$$

It follows that the derivative is positive (negative) when $T_E < 1/2\varepsilon^*$ for a prescribed constant δ positive (negative). In this case, the absolute value of the error ΔF increases with T_E. For larger T_E, the error decreases. A slightly more general result can be found if $\delta = \delta(T_e)$.

Improvements in the solution resolution for high temperature regions in which relatively short time scale processes occur, can be achieved by optimizing the values of *both* Δz and λ relative to a particularly sensitive solution feature. In this work, the time-history of the pressure behind the lead shock is used to obtain refined values of the two parameters, and the results are supported by the associated behavior of $q_{ch}(s)$ defined in (26).

6   Optimization Procedure

Computational solutions for $0 \leq s \leq 40$ have been obtained for the thermal power deposition formula in SKH (Equations 39-42), with $\varepsilon^* = 0.08$, $\hat{B} = 15$, $q = 6$, $\gamma = 1.4$, $C_v = C_p = 1$, for a variety of λ and Δz values. The oscillation amplitude of the post shock pressure relative to the mean value at $s = 40$ has been found. First, results are obtained for $\Delta z = 0.05$ and increasing discrete values of λ, beginning with $\lambda = 0.8$. A pronounced global minimum value is observed at $\lambda = 0.91$ as seen in Fig. 1. Thereafter, results are

24

obtained for a sequence of increasingly small grid sizes down to $\Delta z = 6.25 \times 10^{-3}$, where the relative oscillation amplitude is about 1%. Subsequently, results are obtained at two neighboring values of $\lambda = 0.91$ to show that away from the minimum very slightly larger oscillation amplitudes are found.

The post-shock pressure as a function of time s is given in Fig. 2a,b for a relatively noisy oscillatory solution ($\Delta z = 0.05$, $\lambda = 0.875$) and a more accurate result ($\Delta z = 6.25 \times 10^{-3}$, $\lambda = 0.92$). At $s = 40$ in the latter the mean maximum pressure deviates by less than 1% from the C.J. value, $p_{CJ} = 35.73$. Larger amplitude oscillations and a lower average post-shock pressure are observed in the poorly converged case.

In Fig. 3a,b results are given for the time-history of the global heat release defined in (26) for the two cases in the previous paragraph. Here again there is a significant reduction in the amplitude of the oscillation for the optimized case, and the average value is within a fraction of a percent of the C.J.-value of 83.1.

These results suggest quite strongly that further reductions in spatial discretization at an optimized value of λ would produce additional reductions in the oscillation amplitudes. It is prudent to conclude that the physical long-time relaxation process is smooth rather than oscillatory, and that the small oscillations present in the computational results have a numerical processing origin. In this regard it should be noted that crucial parameters used here, $q = 6$ and $\varepsilon^* = 0.08$, differ markedly from the unstable galloping detonation wave problem studied by Fickett and Wood (1966), more recently by Bourlioux et al. (1991) and many others. There $q = 8.33$, $\varepsilon^* = 0.02$, and a moving piston supports the unstable wave propagation process.

7 Computational Results

The computational results are to be given a thorough physical interpretation in order to elucidate the fundamentally transient reactive gasdynamics occurring as a planar DDT evolves. First, a description is given of events following power deposition into a gas volume isolated from the boundary, where $z_i = 3$ (refer to (10)). Examination of the time-history of the spatial distributions of the dependent variables in (1)-(5), along with the local and global heat release in (25) and (26), provides insights into the roles of shock wave generation and multiple reaction center (hot spot) formation in DDT evolution. Subsequent comparisons with results for $z_i = 2$ and 4 help to quantify the impact of initiating power deposition location on the ensuing reactive gasdynamic transients. Parametric studies for the case $z_i = 2$ are used to quantify effects of the initiating power deposition amplitude and the activation energy of the one-step reaction on the evolution to detonation.

The computational results can be interpreted in the context of the following dimensional quantities;

1. $p_o' = 1$ atm, $T_o = 300$ K, $a_o' = 350$ m/s

2. $\ell' = 0.35$ mm

3. $t_H' = t_A' = 1$ μs

4. $q' = 1.82 \times 10^6$ J/kg, $B' = 1.07 \times 10^7$/s, $\gamma = 1.4$

corresponding to the nondimensional parameters $\hat{B} = 15$ and $q = 6$. The specific heats are assumed to be constants which precludes the excitation of internal modes. In addition, dissociation is not included in the model. As a result, the temperature extremes are larger

than one would see in a typical reactive gas mixture where thermal energy can be absorbed by excitation of rotation, vibration and dissociation of molecules.

Equations (9-12) can be used to find the dimensional initiating power deposition per unit volume,

$$\left(p'_o/t'_A\right) \int_{z_i-2}^{z_i+2} \rho \hat{Q} dz = 1.08 \times 10^{12} f(s) W/m^3 \tag{43}$$

where $f(s)$ is defined in (12). The integration limits in (43) imply that the heated region has a spatial extent of 1.4mm. The duration of the deposition is $10 \mu s$. A time integration of (43) can be carried out to find the total energy deposition per volume, $E'_D = 1.53 \times 10^7 J/m^3$. The inert temperature rise resulting from E'_D is characterized by $O(10^4 K)$.

The numerical results have been obtained with a uniform spatial resolution of $\Delta z = 0.01$, unless otherwise noted.

7.1 The case $z_i = 3$, $\varepsilon^* = 0.0725$

The temporal variation of the nondimensional spatial temperature distribution is given in Fig. 4 for the first few microseconds of the deposition process when $z_i = 3$. Shortly after the initiation of power deposition, lasting to $s = 10$, one observes temperature variation beyond the heated region, $1 \leq z \leq 5$, implying that the an exothermic chemical reaction has been initiated in the neighboring mixture, the result of compression wave propagation from a power deposition region. Nondimensional values of the temperature greater than 10 appear for $s = 2.5$, the result of a combination of external source and chemical heat release (see (23)). In fact, species distributions in Fig.

27

6 at $s = 2$ and 4 show that the reactant in the heated region is totally consumed by the latter time value.

Thermal power absorption and exothermicity in the heated region (see eq. (14)) are the sources of gas motion and compression waves that propagate both to the left and the right. The properties of the integrals in (14) imply the induced local gas Mach number, defined by $M_t = u'/a' = u/T^{1/2}$, is less than one for the source deduced in (9)-(12) when $s \le 10$. Negative velocity values (u) are possible when the localized fluid particle compression $\frac{1}{P}\frac{DP}{DS}$ is sufficiently large. Leftward moving gasdynamic waves reflect from the boundary and move back into the partially or fully reacted, heated mixture. These compression waves steepen into shocks seen in the lower two figures in Fig. 4. The shock Mach number in the latter, based on data at $s = 3.4$ and 3.5 is $M_s \approx 1.3$. The observed temperature jump, $\Delta T \approx 3.4$, is nearly identical to the expected value for an inert shock when $\gamma = 1.4$ (Liepman and Roshko 1957). In contrast the Mach number of the evolving lead shock moving to the right is considerably larger because the sound speed of the cold gas is much lower.

A reaction zone, represented by the relatively large, but smooth temperature gradient, trails the lead shock. It moves relatively slowly compared to the rightward moving shock coming from the left seen in the last inset of Fig. 4 and the first two in Fig. 5. A coalescence process is seen in the latter, leading to the formation of a more sharply defined reaction zone seen in the third and fourth insets of Fig. 5 for $s = 8.1 - 8.6$. The corresponding species result can be seen in the fourth inset of Fig. 6 where the steep

concentration gradients are correlated with steep, but smooth temperature gradients referred to previously.

The large temperature values observed near $z = 5$ in the 3rd and 4th insets of Fig. 5 and the second inset in Fig. 6 result primarily from the magnitude of the externally supplied thermal energy noted below (43). Only a small fraction of the total added energy is actually needed to initiate the reaction since the species profiles in Fig. 6 show that the reactant in the heated region is burned out by $s = 4$, while the external heat addition proceeds until $s = 10$. Later, initiation with reduced levels of external thermal energy is considered.

The larger time temperature distribution results in Fig. 5 and those that follow in the first two insets of Fig. 6 show that about 10μs after the heating is initiated, a combination of reaction processes and inert gasdynamics have caused a shock-generated temperature disturbance out to about $z = 22$. The last two insets in Fig. 6 show that there is an unburned pocket of mixture adjacent to the boundary. To the right, a high temperature region of combustion products is found (see the second inset), delimited by a well defined reaction zone (a deflagration) moving into a gas that has been compressed and heated by a relatively weak lead shock ($\Delta T \approx 2$).

The region between the shock and the reaction zone is not entirely inert. The bumps in the temperature distributions represent the early formation of localized hot spots moving with the gas. The ripples in the species concentrations at $s = 6 - 10$ (Fig. 6, last inset) represent small amounts of reactant consumption in the developing hot spots. It is noted that at $s = 10$ there is more than one ripple (and bump) in the curves, representing

the formation of more than one localized hot spot. This result may be contrasted with that found in SKH where symmetric heating leads to a single isolated reaction center. In the present case of asymmetric heating, gasdynamics waves reflected from the boundary are the presumptive sources of the multiple spots.

Further evolution of two localized hot spots can be observed in the first inset in Fig. 7 where substantial variations in the temperature can be seen between the reaction wave to the left and the inert shock to the right. The corresponding species profiles are shown in the third inset of Fig. 7, where the reactant consumption pattern is clearly discernable.

Subsequently, the hot spots spread and coalesce, produce new compression waves moving to the right and strengthen the lead shock by the time $s = 22$ is seen in the second and fourth insets in Fig. 7. At $s = 18$ one observes largely unburned pockets of reactant adjacent to the wall and near $z = 20$. In addition there is a partially burned region near $z = 27$. Beyond that there is a smooth reaction front in the region $30 \leq z \leq 37$ which separates fully reacted mixture from shocked, unreacted gas. The lead shock is observed to precede the reaction zone by several spatial units.

A few microseconds later, at $s = 20$ the unburned pockets remain, although the second of the two has moved with the gas a few spatial units to the left. The partially burned region now located near $z = 28$ has nearly vanished. Meanwhile, the smooth reaction front has moved to the right approximately 8 spatial units. The right side of the reaction zone, where substantial deviation from $Y = 1$ exists is now at about the same z location as the lead shock. This suggests that the shock has been sufficiently strengthened to enable a relatively fast reaction to exist just behind the discontinuity.

Finally, at $s = 22$ one can observe a significant temperature bump behind the lead shock, representing the appearance of yet another localized hot spot in the field. The analogous species profile in the fourth inset of Fig. 7 shows a relatively steep reaction zone just behind the shock, followed by a partially reacted region near $z = 50$ associated with a lower temperature seen to the left side of the new bump. At this point the detonation wave is nearly formed, defined as a self-sustained wave set consisting of a shock with a coupled reaction zone.

Pressure profiles for the evolving reactive gasdynamic process are shown in Fig. 8. The first inset shows a localized pressure spot at $s = 2$. Further pressure enhancement by heating, subsequent relaxation (gas expansion) and compression wave generation to the left and right lead to the shock dominated structure at $s = 4$. The lead shock moves to the right, followed by the faster shock associated with wave reflection from the boundary. Coalescence is seen in the second inset to occur just after $s = 6$. There follows a period of shock decay because the reaction processes described above are decoupled from the lead wave. In contrast one notes lead shock strengthening in the third inset, as compression waves generated by the evolution of multiple localized hot spots propagate through the gas toward the lead wave. Subsequently, the localized chemical heat deposition just behind the lead wave causes a very rapid enhancement of the lead shock and one sees at $s = 22$ the formation of the pressure profile reminiscent of a transient ZND wave.

The time history of the local chemical heat release rate distributions with z in (25) is given in Fig. 9 for increments of time between 19.6 and 26. The set of small amplitude

31

spikes to the left, representing heat from the combustion of the aforementioned unburned mixture pockets, are considered in more detail in Fig. 10. The largest amplitude profiles represent the consequences of rapid chemical reactions just behind the lead shock. The reaction center in the vicinity of $z = 40$ at $s = 19.6$ evolves into a bifurcated structure at $s = 20.6$, when a new reaction zone appears just behind the strengthened lead shock. The enhanced maximum values reflect the increasing post shock temperatures as the lead shock strengthens. Further evolution of this structure is observed at $s = 21.6$ and 23.0. The shock-coupled reaction zone at the latter time value has separated from the nearly burned-out reaction center. Subsequent profiles are associated with an over-driven, transient detonation.

Figure 10 shows the details of the local heat release distributions for the unburned pockets at four time values (right to left) beginning with $s = 19.6$. The twin local peaks at $s = 19.6$ suggest that most of the reaction is occurring on the edges of the pocket Results at subsequent time values show that the pockets are being convected to the left by the local gas flow. The profile at $s = 26$ indicates that the entire pocket has begun to react, with burnout soon to occur.

Species profile structural features in Fig. 11 correlate with those in Fig. 9 and help to confirm the physical interpretation based on local heat release. The downward spikes in the curves at $s = 20.6$ and 21.6 represent the birth and evolution of a new reaction zone that burns out at larger time values.

Equation (14) is used to produce the global heat release rate curve in Fig. 12 where data are recorded at intervals of $\Delta s = 0.01$. The first local peak is associated with the

reaction initiation process generated by thermal power deposition, represented by the mesa-shaped curve beneath the peak. A subsequent decline in chemical power output is characteristic of the early phase of these DDTs where close coupling of shocks and reaction zones is absent. In the vicinity of $s = 17$, one observes a second local peak arising from the appearance of the multiple reaction centers seen in Fig. 7. The subsequent global maximum is correlated with the appearance of the multiple reaction zones at $s = 20.6$ and 21.6 in Figs. 9 and 11. The rapid decline that follows occurs when only a single reaction zone is coupled to the shock at $s = 22.6$, the result of a sufficiently large shock-induced temperature increase which facilitates very short induction times. The fourth local maximum arises from the delayed combustion of the unburned pockets portrayed in Fig. 10. Finally, the global heat release curve asymptotes (with small oscillations of computational origin) to the steady C.J. value of q_{ch} found from combining (14) with (5) for a steady state wave,

$$q_{ch_{CJ}} = \frac{q}{(\gamma - 1)} M_{CJ} = 83.1 \tag{44}$$

where

$$M_{CJ} = \left[1 + \frac{(\gamma + 1)q}{2}\right]^{1/2} + \left[\frac{(\gamma + 1)q}{2}\right]^{1/2} = 5.54 \tag{45}$$

The corresponding post-shock pressure value, $p_{CJ} = 35.64$.

Global heat release rates per unit area in a shock coupled reaction zone (RZ) can be found from the product of the mass input rate per unit area and the heat of reaction of the reactant. In nondimensional terms (see 1-5),

33

$$q_{RZ} = qM_s / (\gamma - 1) \quad ,$$

where M_s is the shock Mach number. Eq. (44) is found for a CJ wave. Momentarily large values of q_{RZ}, represented by the spike in Fig. 12 imply that either $M_s > M_{CJ}$ or that a multiple reaction zone structure exists, like that seen in Figs. 9 and 11. In fact, the maximum post-shock pressure, seen in Fig. 13, $p \approx 40$ is compatible with a shock Mach number $M_s = 5.87$, which corresponds to $q_{RZ} = 88.01$, only about half of the value found in Fig. 12. This suggests that the multiple reaction zone structure is responsible for the transient heat release spike.

Equation (25) can be differentiated with respect to time to find the conditions for a global maximum in q_{ch} at time s_M. It follows that,

$$\rho_s W_s(s_M) \exp\left[-1/\varepsilon^* T_s\right] = -\int_0^{z_s(s_M)} \frac{\partial}{\partial s}\left[\rho Y \exp\left(-1/\varepsilon^* T\right)\right] d\hat{z} \tag{46}$$

where W_s is the shock Mach number and (ρ_s, T_s) are the postshock density and temperature, both functions of W_s. The integrand represents the time derivative of the rate of reactant consumption. It is noted that the integral must be negative since the lefthandside is positive. It follows that when q_{ch} is maximized, the rate of chemical power production is already declining in the average.

The time dependence of the local pressure maximum is given in Fig. 13 constructed by identifying the largest pressure value in the spatial field at each instant. Lead shock strengthening generates the rapid increase in p_{max} beginning at about $s = 15$. The global maximum at $s = 23.60$, associated with the strongest part of the overdriven detonation formation, has a value approximately 12.12% greater than the subsequent C.J value of

34

35.64. The post-maximum 1.5% "noise" occurs when the spatial resolution is $\Delta z = 0.01$. Further reduction in grid size will diminish the oscillations as the results in Fig. 2 imply. The mean value appears to be asymptoting to the C.J. value on a sufficiently long time scale. One should note that the maximum power level q_{max} occurs at $s = 21.6$, before that for global pressure maximum at $s = 23.60$. This sequence of results is characteristic at many different parameter values, to be discussed in more detail in later sections. This time sequence suggests that compression waves generated by the localized reaction zone during the runup to the heat release maximum propagate forward to the lead shock, maximizing the shock pressure a few acoustic times later.

The spatial distributions of the pressure profiles at the time values in Figs. 9-11 are shown in Fig. 14. The small amplitude disturbances on the left represent relatively weak compression waves propagating toward and reflecting from the planar boundary. The larger profiles to the right show the shock wave strengthening process as the shock-coupled reaction zone evolves a maximum pressure at $s = 23.60$ and a subsequent decline as depicted in Fig. 13.

7.2 The case $z_i = 4$, $\varepsilon^* = 0.0725$

The impact of moving the thermal power deposition region farther away from the bounding wall, to $2 \leq z \leq 6$, can be observed in Figs. 15 and 16. First, it is noted that the general features of the global heat release curve are quite similar to those in Fig. 12 and that the initiation power curves are identical. With the exception of the initial peak in q_{ch} at about $s = 3$, all other local maxima in Fig. 15 occur at a slightly later time In addition, each local maxima is larger than the analogous value in Fig. 12. Finally, the shapes of

the absolute maxima curves are nearly identical, although they occur at different times and have different absolute values. This comparison suggests that the final formation of the overdriven deformation is independent of the earlier initiation process.

Subsequent to the fourth local maximum of q_{ch} at $s \approx 29.5$, due to the heat release from the consumption of the previously unburned pockets, the mean value of the curve asymptotes to the C.J. value of 83.1.

A comparison of results in Figs. 13 and 16 indicates that the absolute maximum pressure is larger and occurs later when $z_i = 4$. Here again, it is observed that the shapes of the primary p_{max} increase with time are nearly identical for much of the rise to the peak. Finally, the pressure peak, associated with the strongest overdriven detonation occurs at $s = 26$, later than that for the absolute q_{max} at 23.8. The noisy pressure relaxation of the lead shock to the C.J. value appears to be slower than that of the global heat release in Fig. 15. Oscillatory behavior observed in Figs. 13 and 16 is a numerical artifact related to issues discussed in Section 4 and described in Figs. 1 and 2.

A comparison of early time temperature distributions for the cases $z_i = 3$ and 4 can be found in Fig. 17a,b. The shocks observed in both cases can be attributed to compression wave reflection from the boundary surface subsequent to the explosion of reactant heated by the initiating power deposition. Shock locations for $z_i = 3$ are beyond $z = 6$ for $s = 4.0$, 4.2 and 4.4. In contrast, when the power deposition is into a region farther from the bounding surface ($z_i = 4$), the shocks are located approximately between $z = 3^-$ and 5.5. It is noted that the shock temperature rises observed in the latter case are within a few

percent of what is expected for a $\gamma = 1.4$ shock moving at the observed local Mach number.

7.3 The case $z_i = 2$.

The detonation initiation process described in this section follows thermal power deposition, defined in (9)-(12), into the region $0 \leq z \leq 4$. This placement of initiating power minimizes the impact of shocks reflected from the bounding surface, in comparison to that in $z_i = 3$ and 4. Results are presented first for $\varepsilon^* = 0.0725$ and varying power deposition amplitudes with the goal of seeking a critical value below which the DDT process is fundamentally altered. Secondly, results at full power are given for several values of ε^* to determine the impact of activation energy on the detonation evolution process.

The global heat release variations with time are given in Figs. 18(a-d) for power deposition levels of 100%, 80%, 60% and 50% when $\varepsilon^* = 0.0725$. The full power result can be compared with that in Fig. 12 for $z_i = 3$ to ascertain the impact of moving the center of power deposition closer to the bounding surface. In particular, the characteristic features in both figures are quite similar, but differ in timing and amplitude. The local maxima occur earlier and have smaller amplitudes when the heated region is closer to the bounding surface. A summary of the full power results in Figs. 12, 15 and 18a is given in Fig. 19, which shows how the amplitude of q_{max} and the time to q_{max} varies with the location of the center point of the heated region z_i. Both appear to be nearly linear for the three z_i-values considered. Altered gasdynamic sequences during the early phases of the event (see Figs. 4 and 5 for examples) are responsible for the observed differences.

The sequence in Fig. 18 shows that decreases in the power deposition amplitude to as small as 50% of the maximum, delay the appearance of the characteristic features and first increases and then decreases their amplitudes. The shape of the q_{max} peak is fundamentally different at 50% of full power. A summary of q_{max} amplitudes and times to q_{max} as functions of initiating power deposition is given in Fig. 20 including data for many input values. When the input power is less than about 63% of maximum, one observes a sharp decline in q_{max}. Concomitantly, the time to q_{max} increases smoothly by more than 100% over the thermal input power range.

These results can be explained by recognizing that a reduced power deposition level leads to a reduced inert temperature rise in the deposition region and a reduced rate of chemical reaction there. The maximum value of the initial peak in the global heat release declines in (a)-(d) as a result. The increasingly weak gasdynamic response leads to a delay in the detonation formation process.

The global maximum pressure variation with time is given in Fig. 21a-d for the range of power input levels in Fig. 18. In general, the absolute maximum pressure (of the lead shock) increases as the power input level decreases while the time to that value increases. These results are summarized in Fig. 22, along with the time to q_{max}. There appears to be a change in character for the p_{max} time when thermal power input is less than about 55% of the maximum value. It should be noted that the time to q_{max} precedes the time to the absolute maximum pressure, $p_{max(abs)}$, until the power level declines to about 57% where a crossover occurs.

38

Local heat release profiles for 100% power deposition are given in Fig. 23 for a sequence of times during which q_{max} occurs at $s = 18.8$, the absolute pressure maximum, $p_{max(abs)}$ occurs at $s = 21.4$ and the overdriven detonation is born. The sequence is very similar to that for $z_i = 3$ described in Fig. 9, including the appearance of multiple zones of energy release. The q_{max} occurs when the original reaction center and the shock-attached reaction zone are both generating chemical heat. In contrast, $p_{max(abs)}$ occurs later when the only substantive heat release is occurring in the shock-coupled reaction zone associated with a transient overdriven detonation.

Species concentration profiles in Fig. 24 help to confirm the reaction zone structures seen in Fig. 23. The sequence of curves on the right side show how a new reaction zone appears spontaneously at $s = 17.8$. The trailing reaction zone burns out at $s \approx 22.4$. In Fig. 25, the pressure distributions with z are given for the same time sequence. The emergence of an unsteady ZND structure is observed, driven by the heat release from the shock-coupled reaction zone.

The impact of activation energy on the detonation initiation process can be observed in Fig. 26a-d where the global heat release, q, versus time is given for $\dot{\varepsilon} = 0.0725$, 0.0750, 0.0775 and 0.0800 when $z_i = 2$ and the initiation power is 100%. A decrease in the activation energy (increase in $\dot{\varepsilon}$) is correlated with a reduction in the global q_{max} and its occurrence at a relatively earlier time.

The final local maximum, associated with chemical heat release from the combustion of the unburned pocket, is observed to occur closer to the time for q_{max} as $\dot{\varepsilon}$ increases. A significant change in behavior occurs when $\dot{\varepsilon} = 0.0775$. The unburned pocket is

consumed during the period of most intense heat release and detonation formation. As a result, the fourth local maximum disappears.

The value of $p_{max(abs)}$ in Fig. 27a-d declines and occurs sooner as $\overset{*}{\varepsilon}$ increases. When $\overset{*}{\varepsilon} < 0.08$ the absolute maximum pressure exceeds the C.J. value and p_{max} approaches the C.J.-value from above. The solution properties change at $\overset{*}{\varepsilon} = 0.08$ where the maximum, mean shockfront pressure rises monotonically toward the C.J. value from below. The reduction in the global heat release maximum seen in Fig. 26 is compatible with reduced compression wave generation and lesser front shock wave enhancement.

The increase in q_{max} with decreasing ε^*, seen in Fig. 28 can be rationalized qualitatively by employing the thermal gradient concept (spatial gradient in the induction time) (Zeldovich et. al, 1970 and Zeldovich, 1980). A reactive mixture fluid particle compressed and heated by passage of the lead shock releases most of its chemical energy in a brief burst of power within a thin reaction zone at the end of the much longer induction zone, the result of the exponential dependence of reaction rate on temperature (Kassoy, 1977). Higher activation energy mixtures are characterized by relatively long induction periods. Extended induction periods imply that a relatively large mass of nearly unreacted mixture can be present behind the shock in a higher activation energy system. During a period of shock strengthening, seen in Figs.13 and 14, the induction time for a sequence of neighboring fluid particles is actually reduced, leading to possibility of multiple reaction zones seen in Fig. 11. Figure 28 also shows increasing values of post-shock pressure, $p_{max(abs)}$ with decreasing ε^*, the result of enhanced local chemical power deposition with increases in activation energy. Concomitant compression

wave generation leads to lead shock strength enhancement. Irregular location of some numerical data points arise from sensitivity to the sampling process.

A nearly monotonic linear increase of the time to q_{max} with decrease in ε^* is observed in Fig. 29, a logical outcome of the lengthened induction time with increasing activation energy. The time to $p_{max(abs)}$ has a minimum near $\varepsilon^* = 0.078$, with a very large increase for further decreases in ε^*. This can be interpreted to mean that when the chemical power deposition level falls below a critical value (see Fig. 26 c and d), the compression wave generation process cannot enhance the lead shock strength beyond the C.J. value (see Fig. 27d).

8 Conclusions

The essential properties of detonation initiation transients are described for stable, planar detonation. The results described in the present work and that in SKH suggest that the transient dynamics of stable, planar DDT evolution are:

1. dependent on the characteristics of the initial power absorption process, including the location relative to boundaries present,

2. quite sensitive to the activation energy for a given level of power deposition,

3. characterized by the spontaneous appearance of several localized hot spots (reaction centers) resulting from the conditioning of isolated volumes of reactive mixture by the complex compression wave structure inherent in a compressible system with thermal power addition from external and chemical sources, and is

4. likely to lead to an overdriven detonation which relaxes smoothly to a C.J. wave, unless the activation energy, E', is sufficiently small. The overdrive is relatively

small in terms of the maximum post-shock pressure and lead shock Mach number, although the global heat release rate peak is significantly larger than the C.J. value for a steady wave. Multiple reaction zone combustion, facilitated by continuous reduction in the induction time of a sequence of reactive fluid particles passing through a continually strengthening shock wave, can account for the observed heat release dynamics. For example, the distance traveled from the shock by an nth fluid particle during the induction time is characterized by $Z_n = \sigma_{in}\sigma_n$ where σ_{in} is the induction time for that particle and σ_n is a measure of the post shock speed relative to the shock. Both quantities are declining with increasing shock strength. It follows that the location of large heat release for a large n particle can be closer to the shock than that for a small n particle, and both can occur at the same time.

The optimization study shows that the small oscillations seen in the SKH results during the overdriven detonation relaxation process to a steady C.J. wave can be systematically reduced by the proper choice of the $(\varDelta z, \lambda)$ combination. The optimized values have been employed for the asymmetric power deposition DDT results described in the present work.

7 Acknowledgements

References

Book DL, Boris JP, Hain K. 1975. Flux-corrected transport II. Generalizations of the method. J. Comput. Phys 18:248-283.

Bourlioux A, Majda AJ, Roytburd V. 1991. Theoretical and numerical structure for unstable, one-dimensional deformations. SIAM J. App. Math 51:303-343.

Clarke JF, Kassoy DR, Meharzi NE, Riley N, Vasantha R. 1990. On the evolution of plane detonations. Proc. Roy. Soc. London A429:259-283.

Clarke JF, Kassoy DR, Riley N. 1986. On the direct initiation of a plane detonation wave. Proc. Roy. Soc. London A408:129-148.

Clarke JF, Kassoy DR, Riley N. 1984b. Shocks generated in a confined gas due to rapid heat addition at the boundary, II. Strong shock waves. Proc. Roy. Soc. London A393:331-351.

Dold JW, Short M, Clarke JF, Nikiforakis N. 1995. Accumulating sequence of ignitions from a propagating pulse. Comb. Flame 100:465-473.

Eckett CA, Quirk JJ, Shepherd JE. 2000. The role of unsteadiness in direct initiation of gaseous detonations. J. Fluid Mech. 421:147-183.

Fickett, WF and Davis, W. 1979, *Detonation*, University of California Press, Berkeley, CA.

Fickett W and Wood WW. 1966. Flow calculations for pulsating one-dimensional detonations. Phys. Fluids 9:903-916.

Gamezo, VN, Desbordes, D and Oran, E. 1999. Formation and evolution of two-dimensional cellular detonations. Combustion and Flame 116:154-165.

Gu XJ, Emerson DR, Bradley D. 2003. Modes of reaction front propagation from hot spots. Comb. Flame 133:63-74.

Kapila AK, Schwendeman DW, Quirk JJ, Hawa T. 2002. Mechanisms of detonation formation due to a temperature gradient. Comb. Theory Modeling 6:533-594.

Kasimov, AR and Stewart, DS. 2004. On the dynamics of self-sustained one-dimensional detonations; A numerical study of the shock-attached flame. Phys. Fluids, 16:3566-3578.

Kassoy DR. 1977. The supercritical spatially homogeneous thermal explosion: Initiation to completion. Q. Jl. Mech. Appl. Math. 30:71-89

Kassoy DR, Kuehn JA, Nabity MW, Clarke JF. 2005. Modeling deformation initiation on the microsecond time scale. AIAA 2005-1169, 43rd Aerospace Sciences Meeting and Exhibit, Reno, NV.

Kassoy, DR and Palaniswamy, S. 2002. Detonation initiation and evolution in a model of a pulsed detonation engine. AIAA 2002-0612, 40th Aerospace Sciences Meeting and Exhibit, 14-17 January 2002, Reno NV.

Khokhov, AM and Oran, ES. 1999. Numerical simulation of detonation interaction in a flame brush: The role of hot spots. Combustion and Flame 119:400-416.

Khokhlov, AM, Oran, ES, and Thomas, GO. 1999. Numerical simulation of deflagration-to-detonation transition: The role of shock flame interactions in turbulent flames. Combustion and Flame 117:323-339.

Lee, JHS. 1984. Dynamic parameters of gaseous detonations. Ann. Revs. of Fluid Mechs. 16:311-336.

Lee, HI and Stewart, DS. 1990. Calculation of linear detonation instability, one-dimensional instability of a plane detonation. J. Fluid Mech. 216:103-132.

Liepman HW, Roshko A. 1957. *Elements of Gasdynamics*, J. Wiley & Sons, Inc., New York.

MacCormack RW. 1969. The effect of viscosity in hypervelocity impact cratering. AIAA Paper 69-354, AIAA Meeting, Cincinnati, OH.

Mazaheri K. 1997. Mechanism of the onset of detonation in direct initiation [dissertation]. Montreal, Canada: McGill University.

Meyer JW, Oppenheim AK. 1971. On the shock induced ignition of explosive gases. 13th Symp. (Int'l) on Combustion, The Comb. Inst 13:1153-1164.

Moen, IO., Donato, M, Knystautas, M and Lee, JHS. 1980. Flame acceleration due to turbulence produced by obstacles. Combustion and Flame 39:21-32.

Nikiforakis N, Clarke JF. 1996. Quasi-steady structures in the two-dimensional initiation of detonations. Proc. R. Soc. London A452:2023-2042.

Oppenheim AK. 1985. Dynamic features of combustion. Phil. Trans. R. Soc. London A315:471-508.

Oppenheim, AK and Soloukhin, RI. 1973. Experiments in gasdynamics. Ann. Revs. of Fluid Mechs. 5:31-55.

Schauer, FR, Miser, CL, Tucker, KC, Badley, RP. and Hoke, JL. 2005. Detonation initiation of hydrocarbon-air mixtures in a pulsed detonation engine. AIAA 2005-1343, 43rd Aerospace Sciences Meeting and Exhibit, 10-23January2005, Reno, NV.

Sharpe, GJ. 2001. Transverse waves in numerical simulations of cellular detonations. J. Fluid Mech. 447:31-51.

Sharpe, G J. 1997. Linear stability theory of idealized detonations. Proc. R. Soc. Lond. A453:2603-2625.

Sharpe, GJ. and Falle, SAEG. 1999. One-dimensional numerical simulations of idealized detonations. Pro. R. Soc. Lond.A 455:1203-1214.

Sharpe, GJ. and Falle, SAEG. 2001. Numerical simulations of pulsating detonations. Part 1, nonlinear stability of steady detonations. Combustion Theory and Modeling 4:557-574.

Sileem AA, Kassoy DR, Hayashi AK. 1991. Thermally initiated detonation through deflagration to detonation transition. Proc. Roy. Soc. London A435:459-482.

Sileem AA. 1989. Initiation and propagation of shock and detonation waves in gases due to power deposition [dissertation]. Boulder (CO): University of Colorado.

Singh G, Clarke JF. 1991. Transient phenomena in the initiation of a mechanically drive plane detonation. Proc. R. Soc. London A435:459-482.

Smirnov NN, Panfilov II. 1995. Deflagration to detonation transition in combustible gas mixtures. Comb. Flame 101:91-100.

Stewart, DS and Kasimov, AR. 2006. The state of the detonation stability theory and its application to propulstion. J. Prop. Power, to appear.

Tegner, J and Sjögreen, B. 2002. Numerical investigation of deflagration to detonation transitions. Combustion Science and Technology 174(8):153-186.

Zeldovich YB, Librovich VB, Makhviladze GM, Sivashinsky GI. 1970. On the development of detonation in a non-uniformly preheated gas. 1970. Astronautic Acta 15:313-321.

Zeldovich YB. 1980. Regime classification of an exothermic reaction with nonuniform initial conditions. Comb. Flame 39:211-214.

Figures
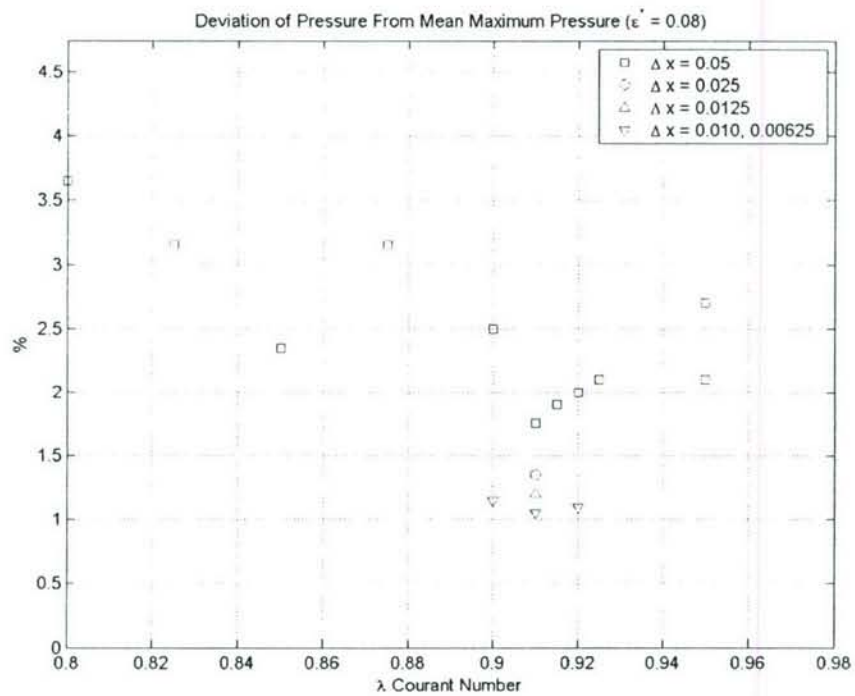
Figure 1. Relative post-shock pressure oscillation amplitude (%) vs. Courant number (λ) with respect to the grid size (Δz) for SKH parameters.
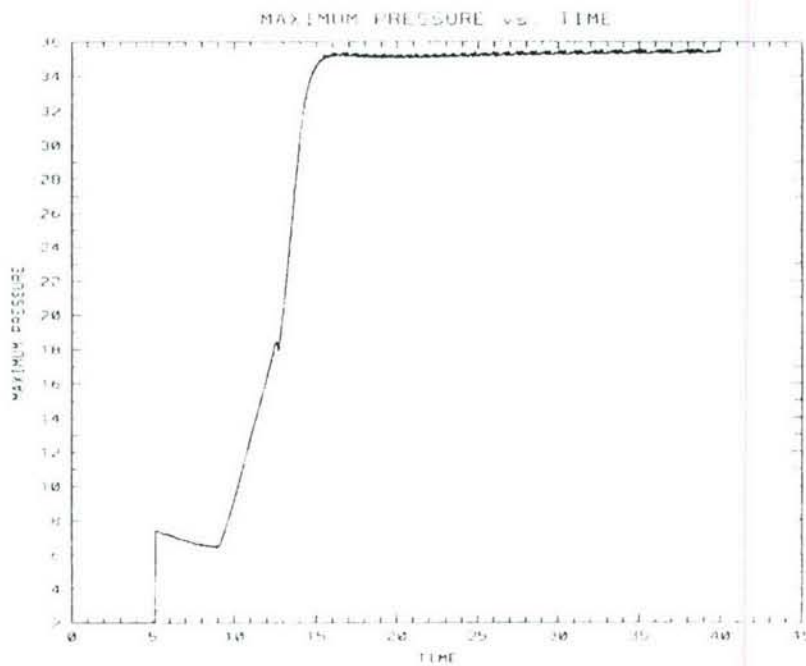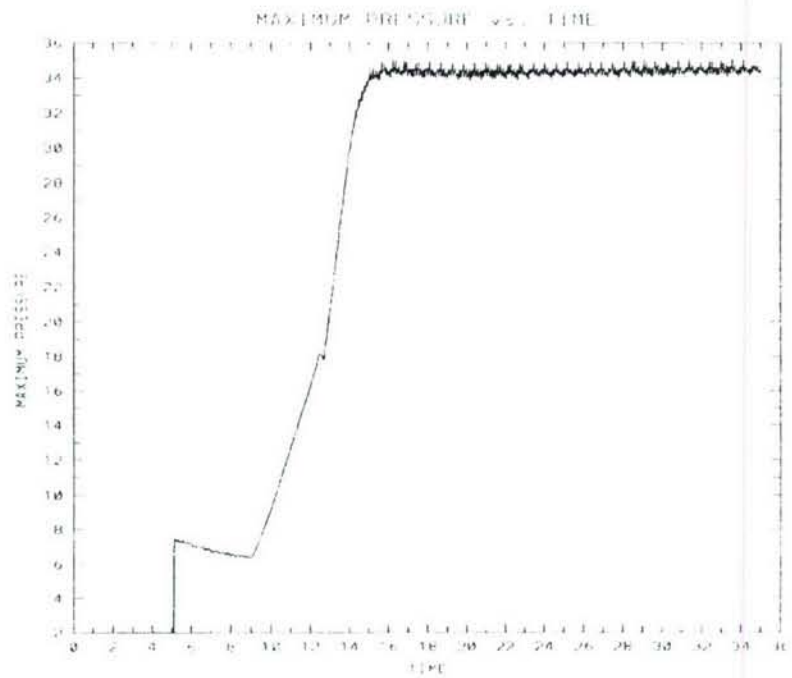
Figure 2. The post-shock pressure variation with time for a poorly resolved case (a), and a more accurate result (b), using SKH data.
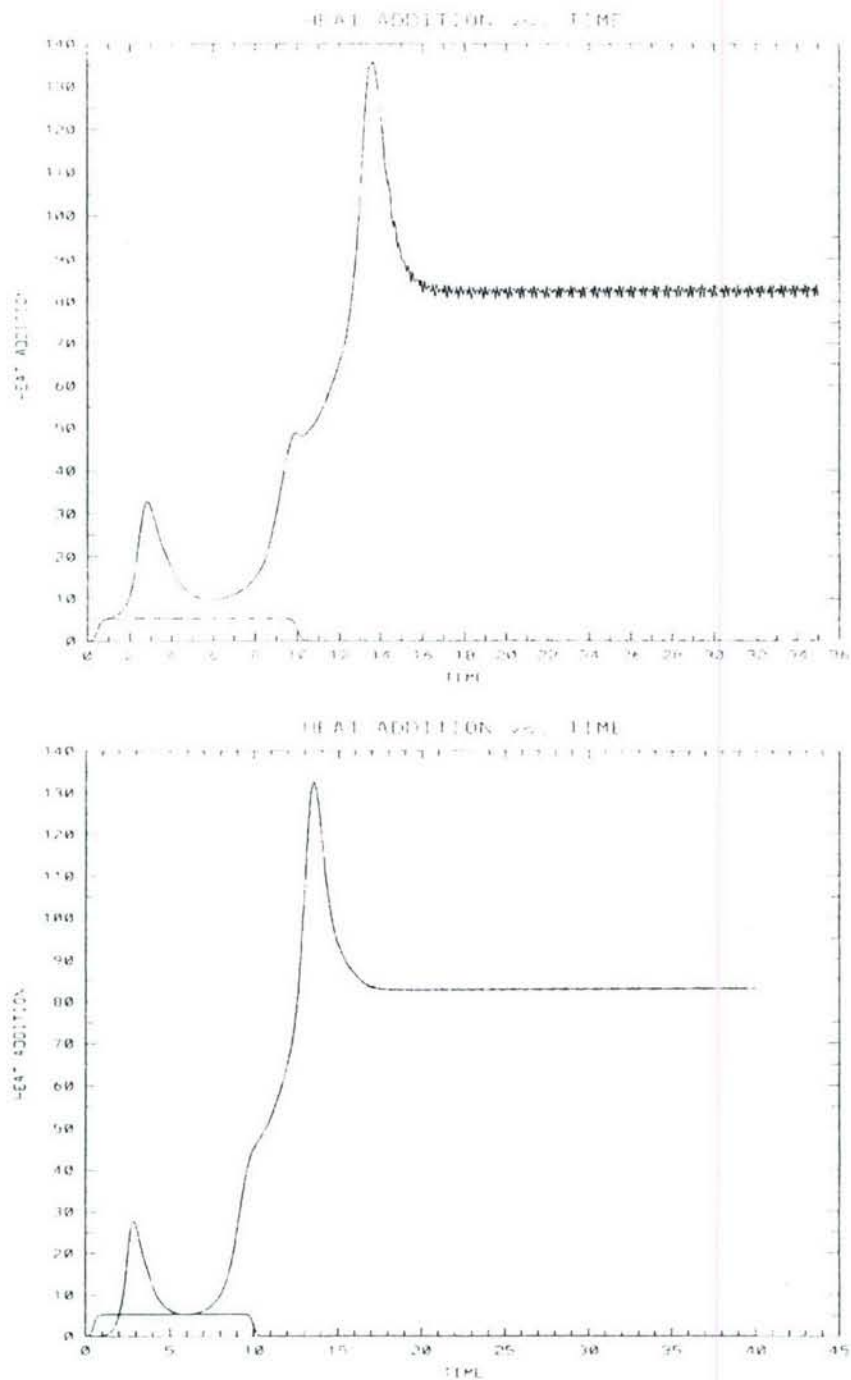
Figure 3. The global heat release variation with time for a poorly resolved case (a), and a more accurate result (b), using SKH data.
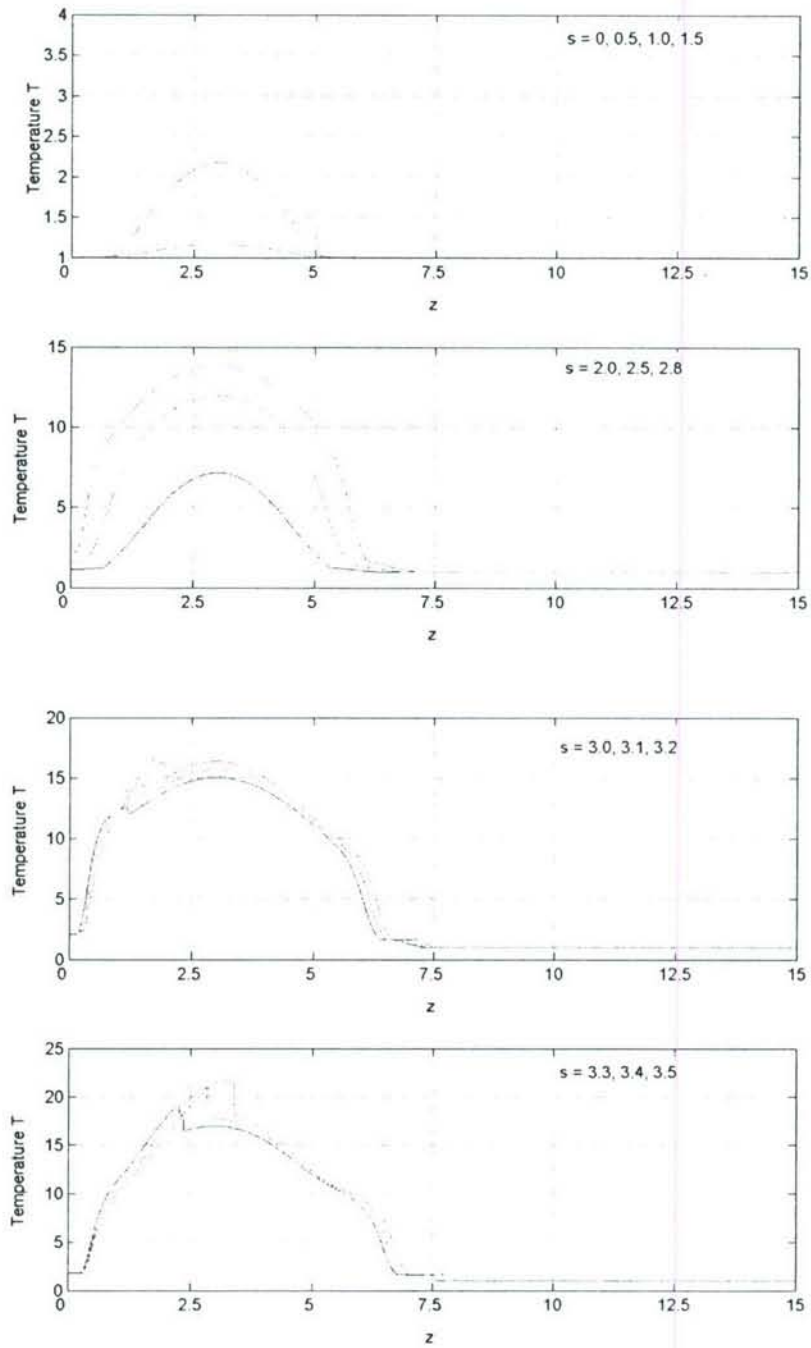
Figure 4. The spatial temperature distribution for several time values to s = 3.5 for $z_i = 3$ and $\varepsilon^* = 0.0725$.
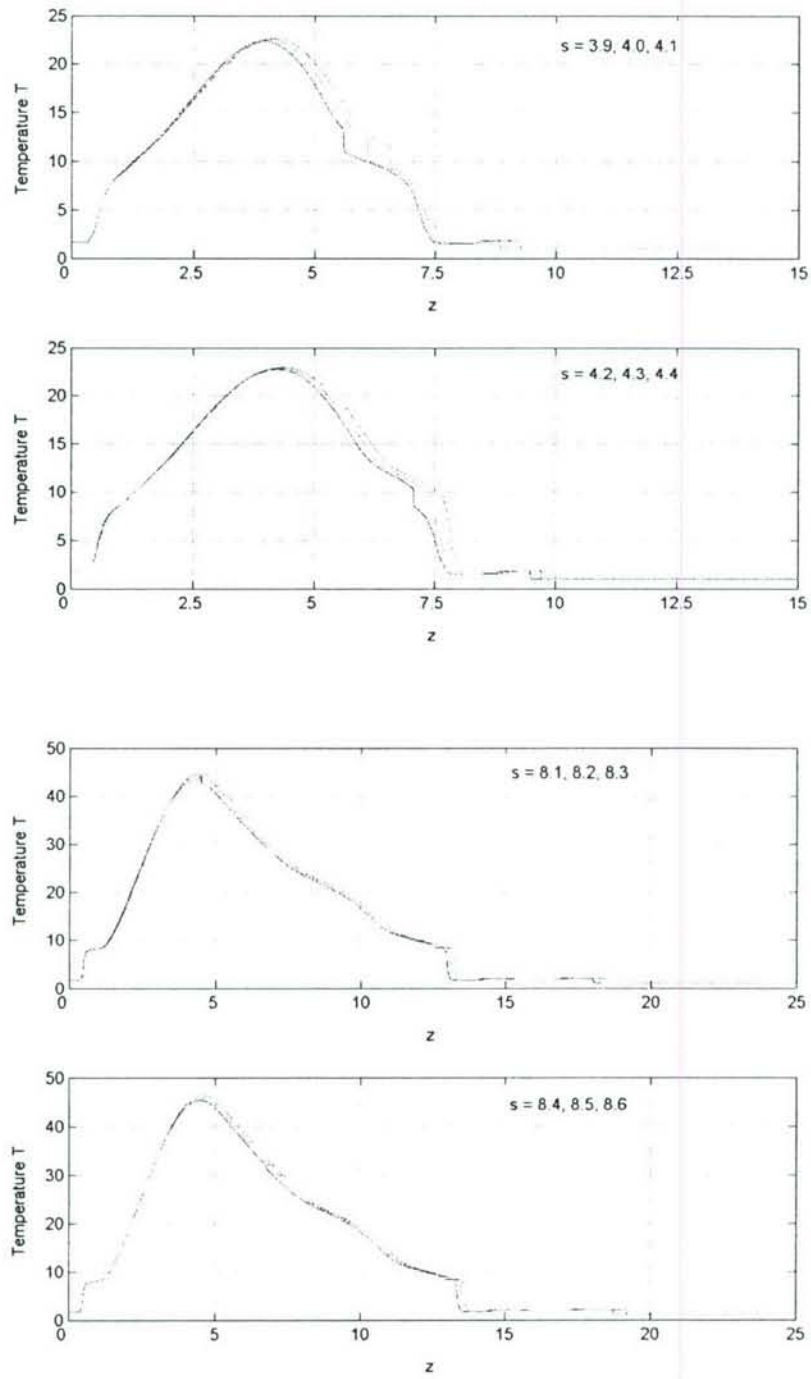
Figure 5. The spatial temperature distribution for several time values from s=3.9 to s = 8.6 for $z_i = 3$ and $\varepsilon^* = 0.0725$.
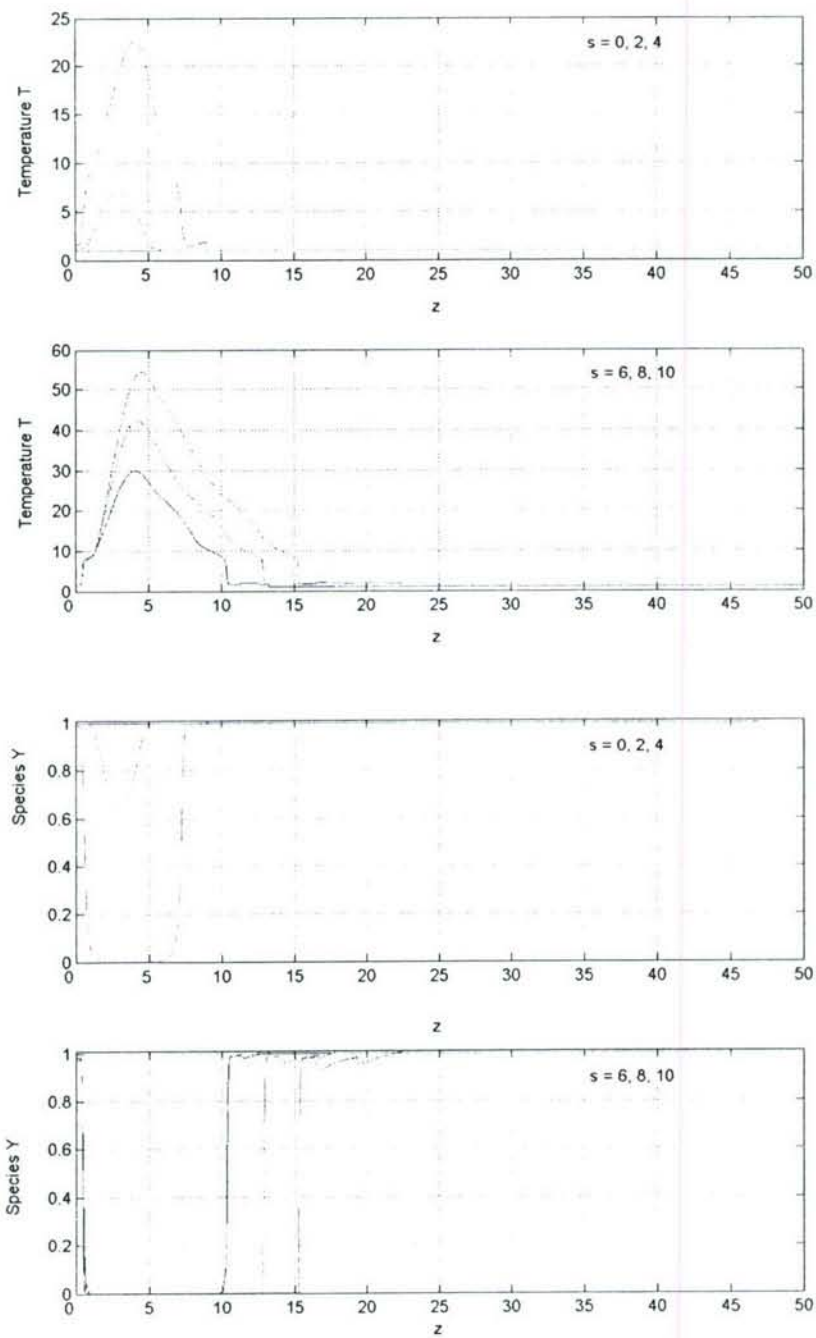
Figure 6. The spatial temperature and species distributions for several time values to s = 10 for z_i = 3 and ε^* = 0.0725.
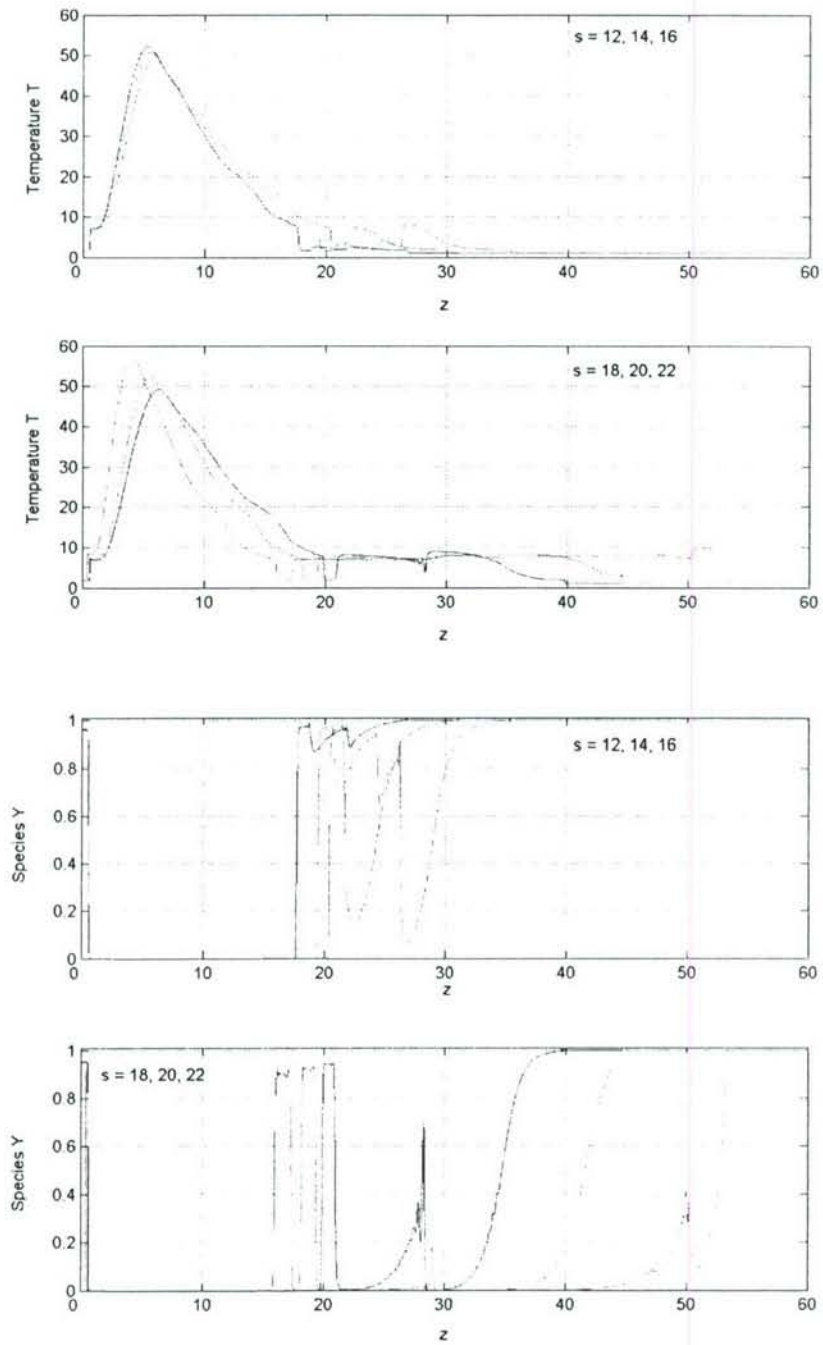
Figure 7. The spatial temperature and species distributions for several time values from s = 12 to s = 22 for z_i = 3 and ε^* = 0.0725
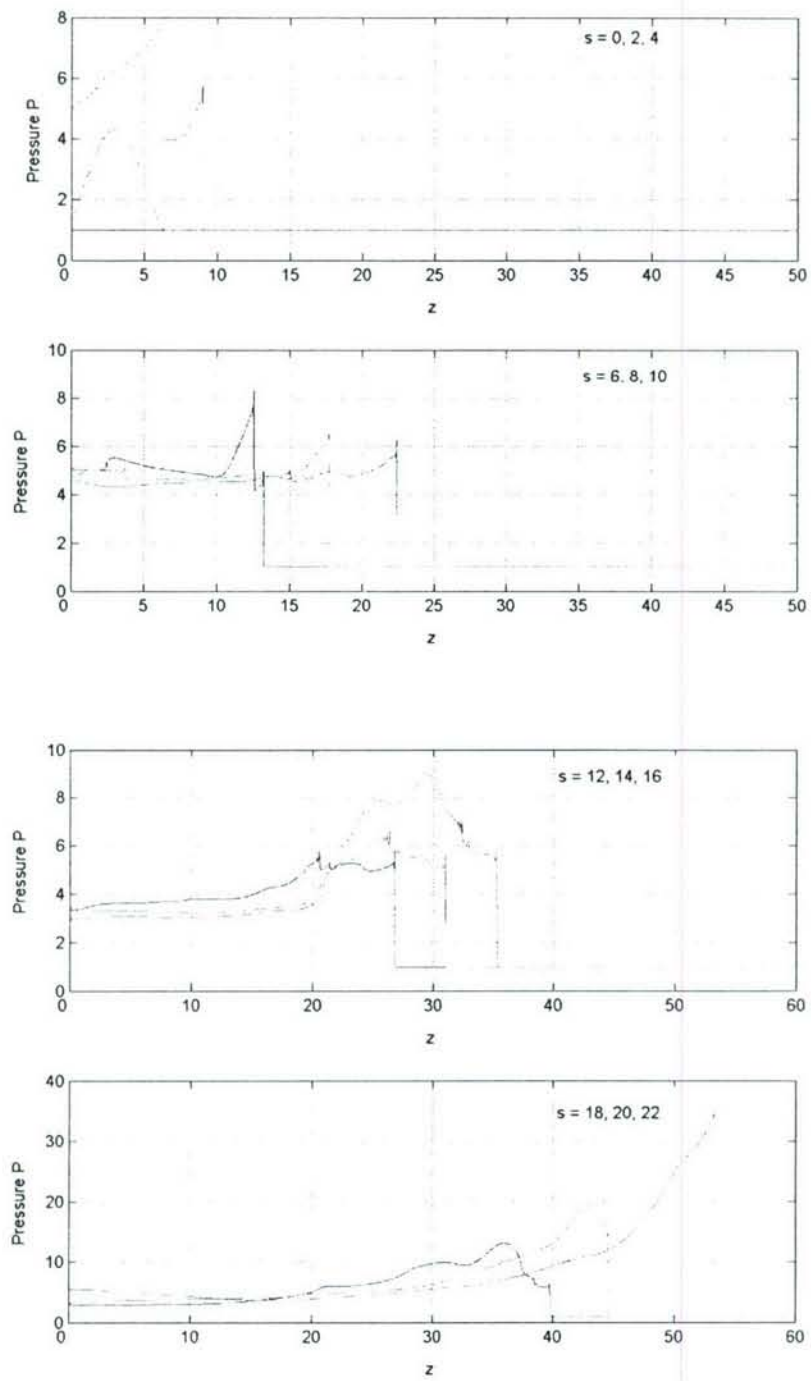
Figure 8. The spatial pressure distributions for several time values to s = 22 for z_i = 3 and ε^* = 0.0725.
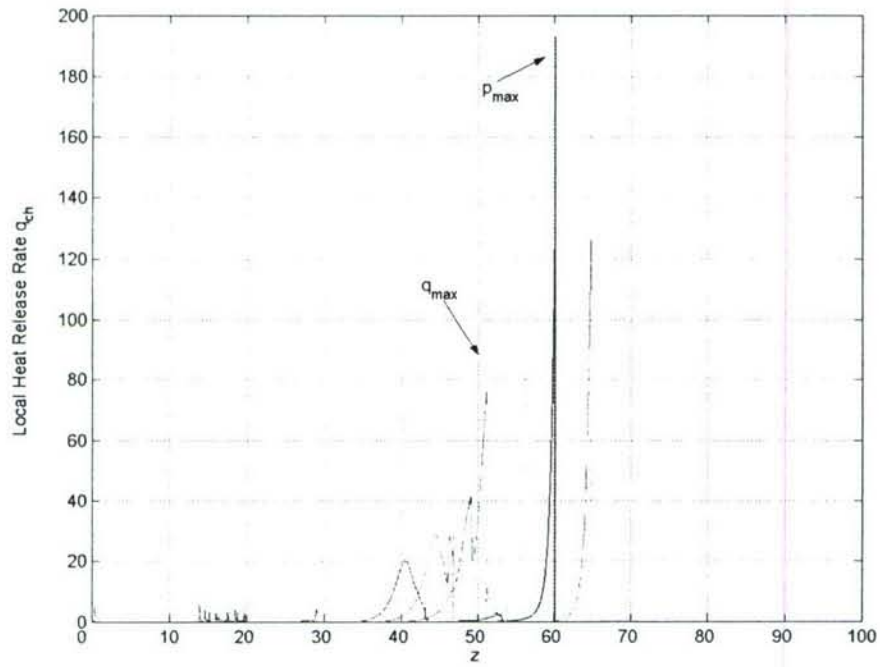
Figure 9. The time history of the local chemical heat release distributions with z, defined in Eq. 25, for the time values s = 19.6, 20.6, 21.6, 23, 24, 25 and 26 when $z_i=3$ and $\varepsilon^* = 0.0725$.
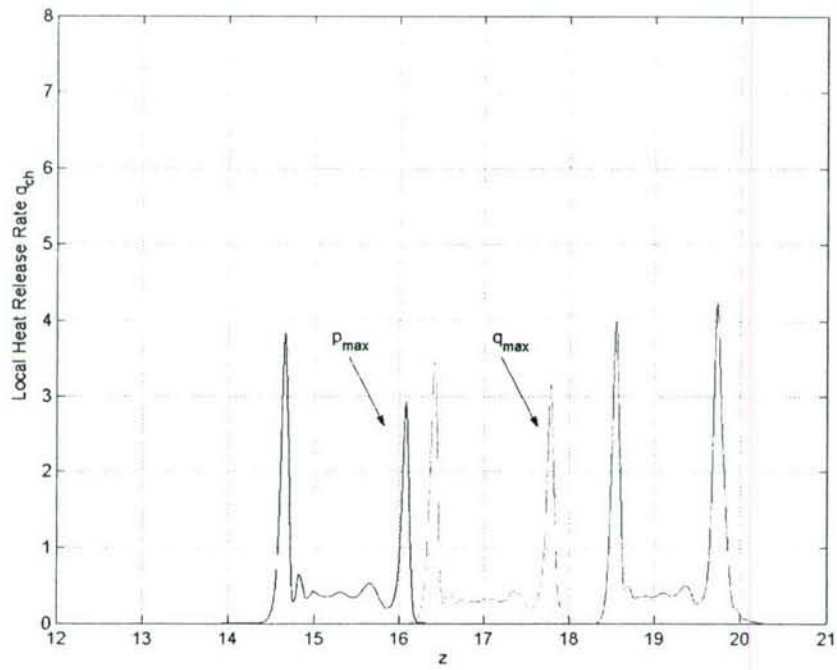
Figure 10. The time history of the local chemical heat release distributions with z in the unburned mixture pockets for the time values s = 19.6, 21.6, 24 and 26 (right to left) when $z_i = 3$ and $\varepsilon^* = 0.0725$.
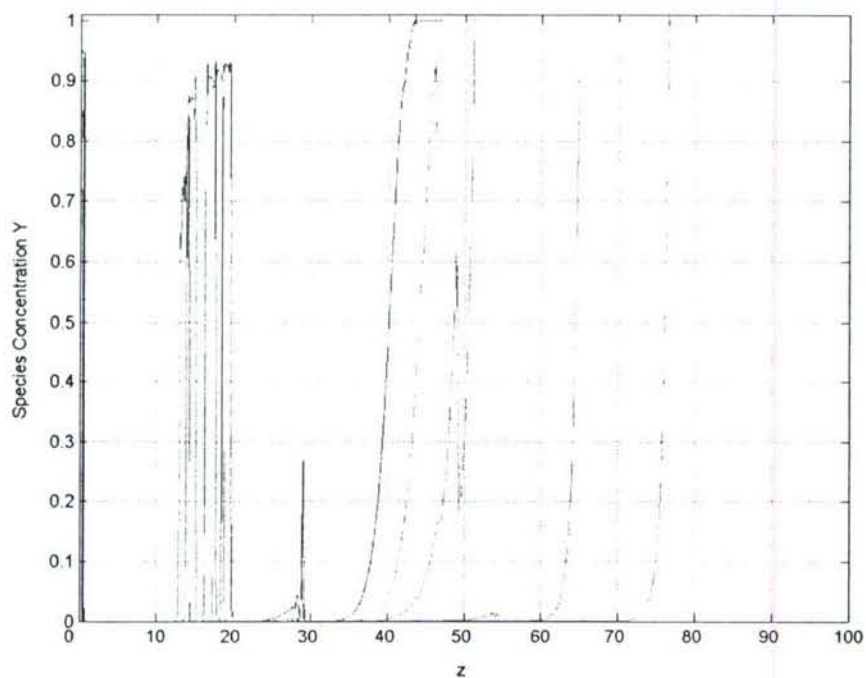
Figure 11. The time history of the species distribution with z for the
time values s = 19.6, 20.6, 21.6, 23, 24, 25, and 26 when z_i = 3 and ε^*
= 0.0725. The seven curves beyond z ≈ 25 are read left to right with
increasing time. The unburned mixture pockets move to the left as
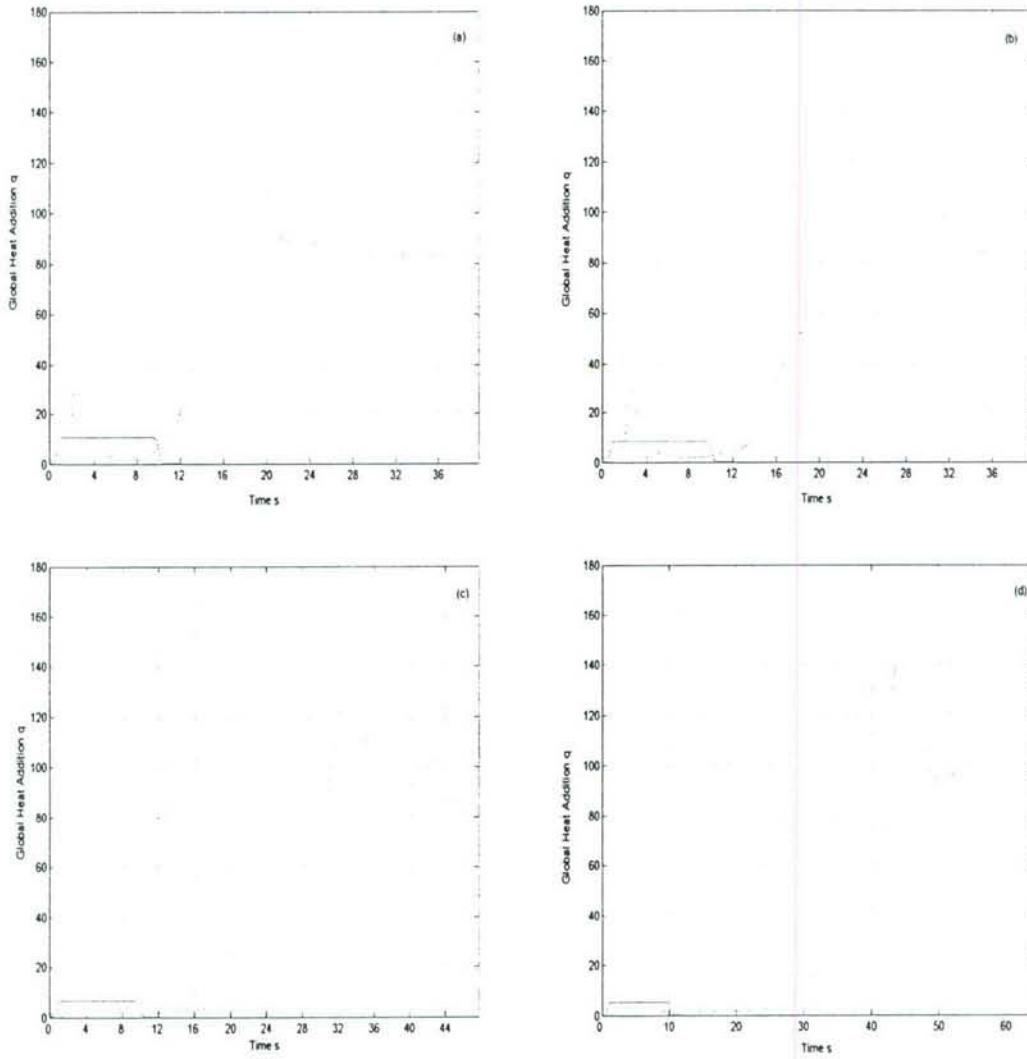time increases.
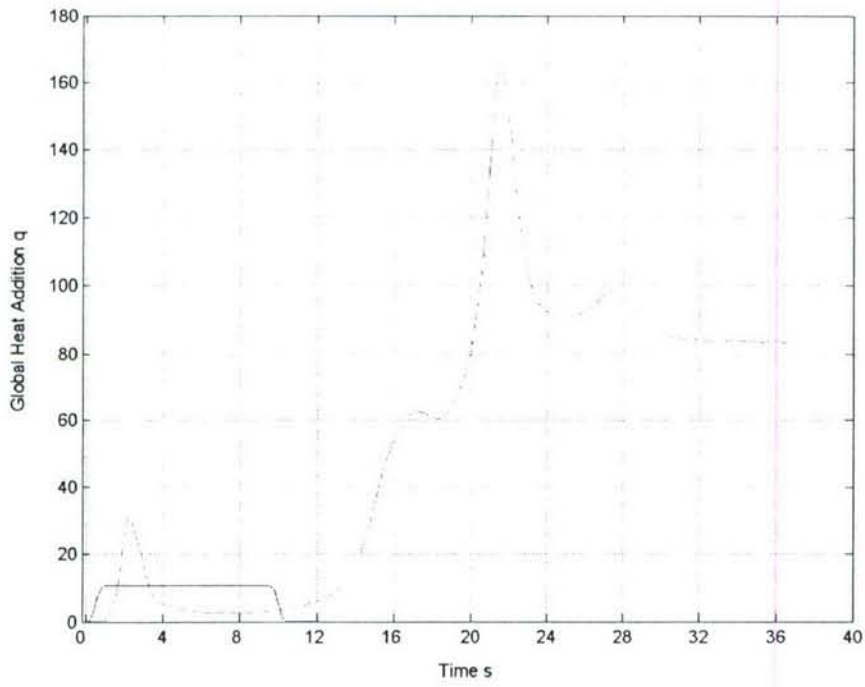
Figure 12. The evolution of the global heat release with time, defined in Eq. 26, exhibiting four local maxima and asymptoting to the C.J. value for a steady detonation wave for $z_i = 3$ and $\varepsilon^* = 0.0725$. The mesa-like curve in the lower left hand corner represents the initial power deposition. The absolute maximum global heat release, $q_{max} = 166.08$, occurs at $s \approx 21.6$.
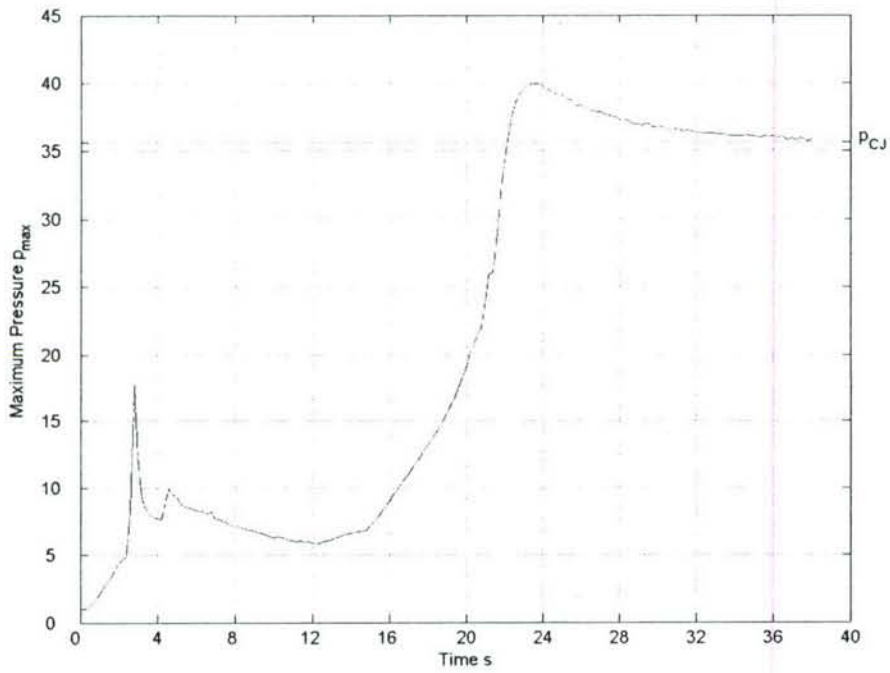
Figure 13. The time dependence of the instantaneous global maximum pressure, p_{max}, corresponding to the appearance of an overdriven detonation and subsequent relaxation to the C.J. value for a steady detonation wave, for $z_i = 3$ and $\varepsilon^* = 0.0725$. The absolute maximum pressure, $p_{max} = 39.96$, occurs at $s \approx 23.6$.
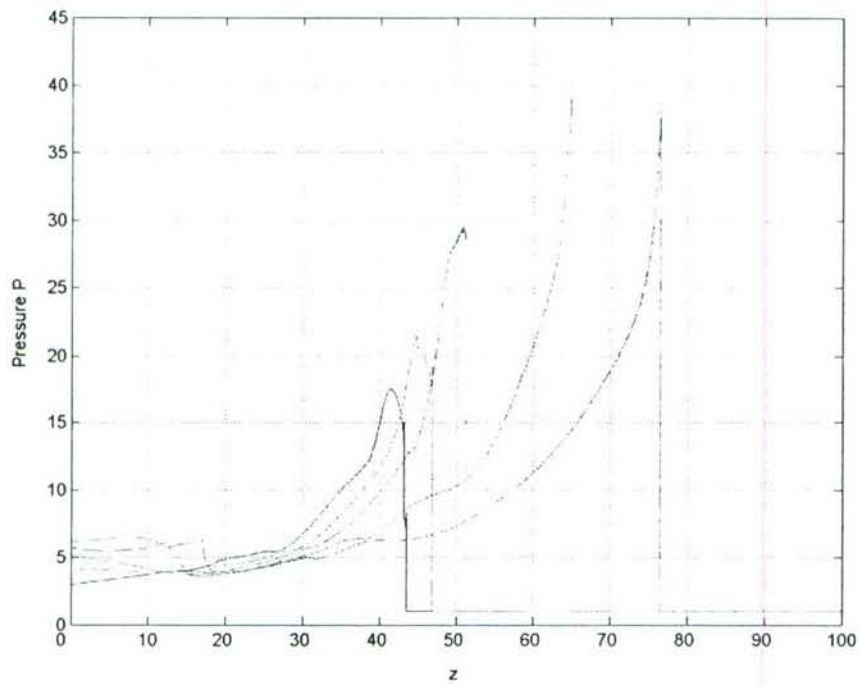
Figure 14. The time history of the pressure distributions with z
for the time values s = 19.6, 20.6, 21.6, 23, 24, 25, and 26 when
z_i = 3 and ε^* = 0.0725, including the effect of relatively weak
compressions reflecting from the wall.
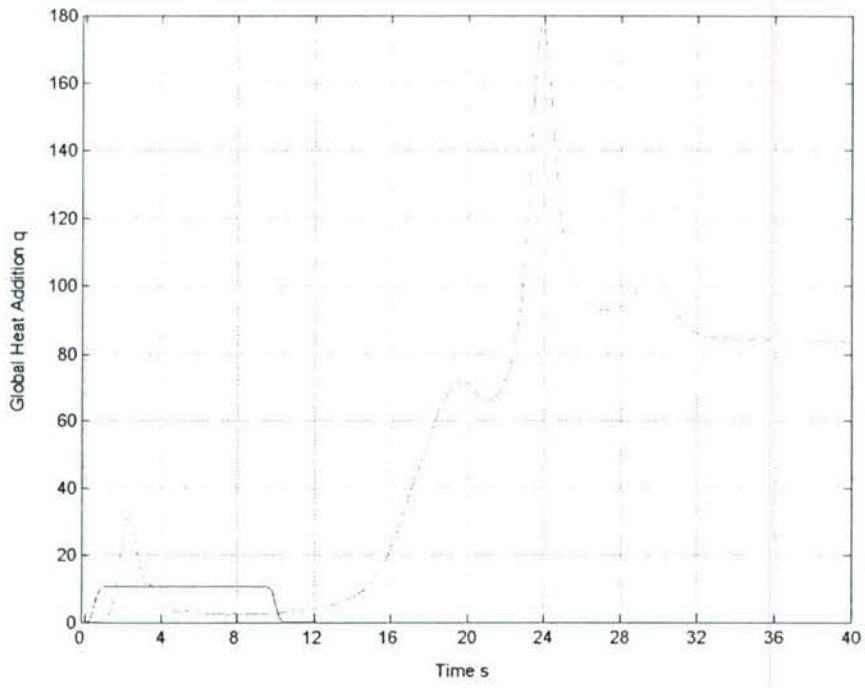
Figure 15. The evolution of the global heat release with time, defined in Eq. 26, when $z_i=4$ and $\varepsilon^* = 0.0725$. The absolute global maximum heat addition, $q_{max} = 176.61$, occurs at $s = 23.8$.
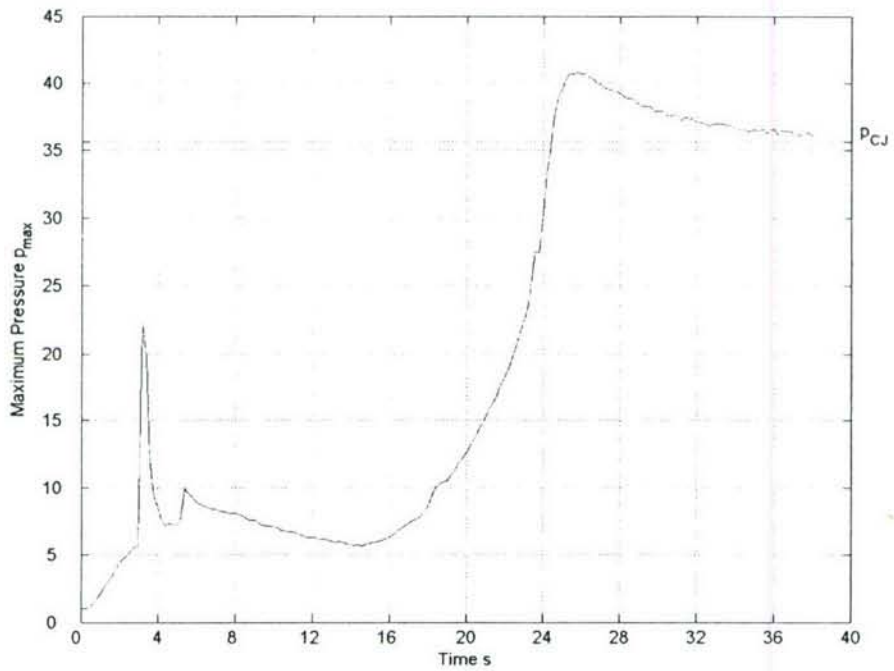
Figure 16. The time dependence of the instantaneous global maximum pressure, p_{max}, corresponding to the appearance of an overdriven detonation and subsequent relaxation to the C.J. val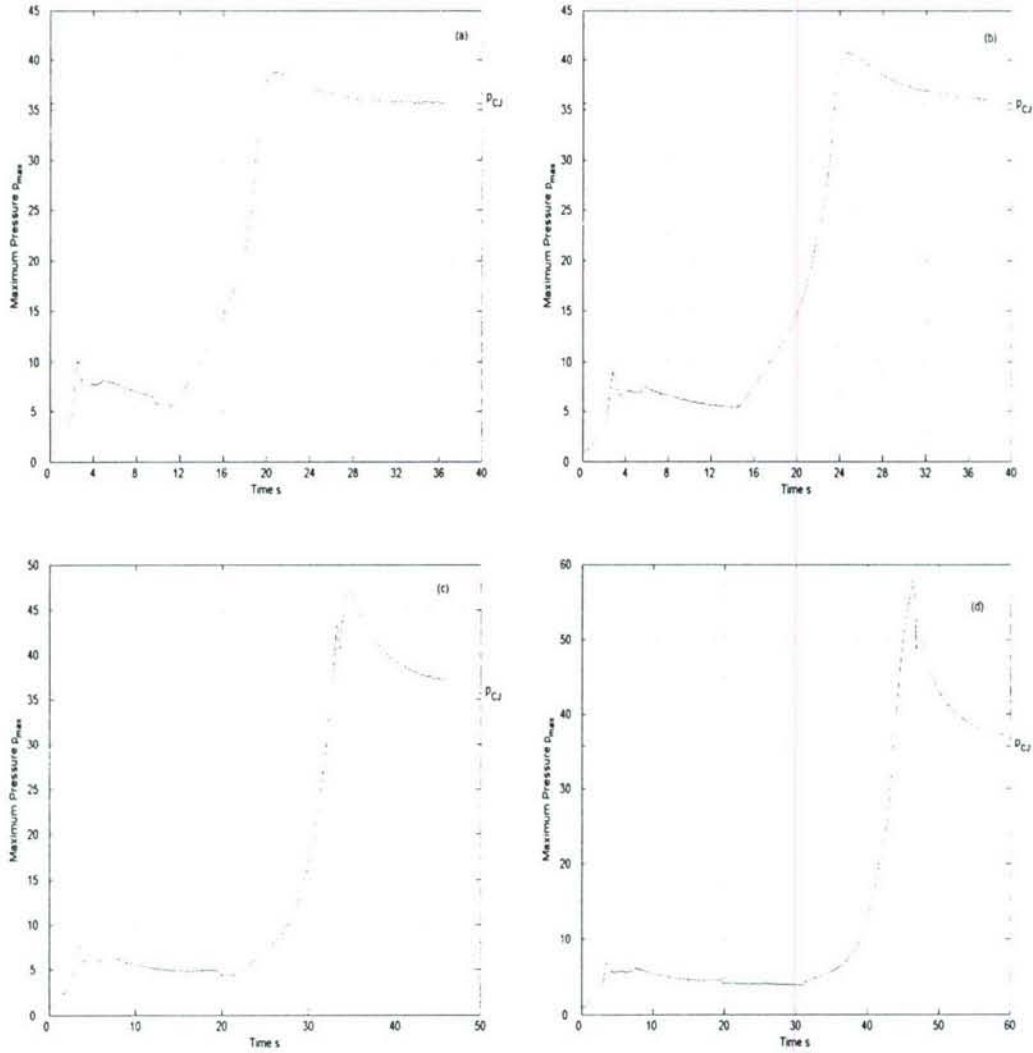ue for a steady detonation wave when $z_i=4$ and $\varepsilon^* = 0.0725$. The absolute pressure maximum, $p_{max} = 40.78$, occurs at $s \approx 25.8$.
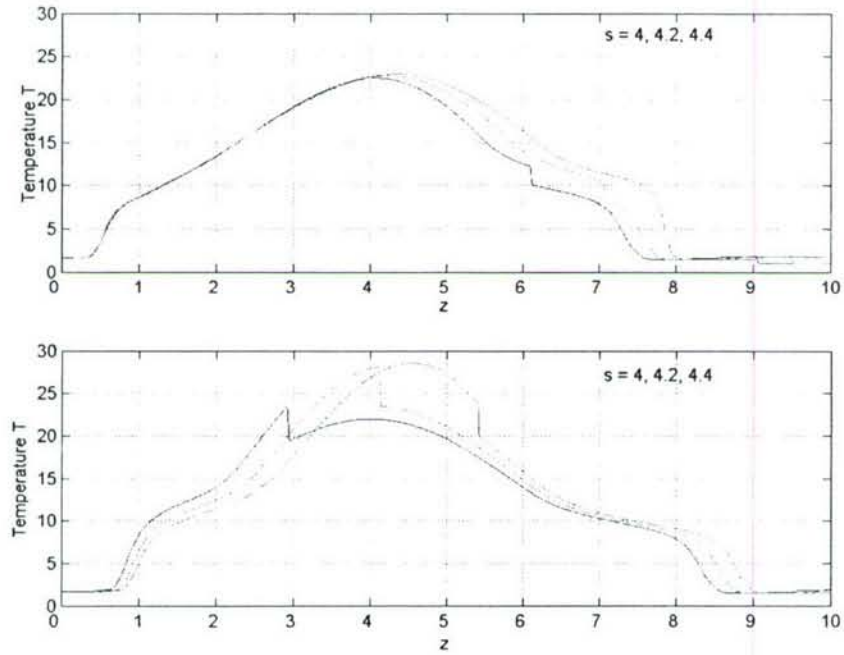
Figure 17. The time history of the spatial temperature distributions with z to show impact of the initial power deposition location when $\varepsilon^* = 0.0725$: a. $z_i=3$, s=4.0, 4.2 and 4.4; b. $z_i=4$, s=4.0, 4.2 and 4.4.

Figure 18. The evolution of the global heat release with time, defined in Eq. 26, exhibiting four local maxima and asymptoting to the C.J. value for a steady detonation wave when $z_i = 2$ and $\varepsilon^* = 0.0725$. The mesa-like curve in the lower left hand corner represents the initial power deposition: a. 100% power deposition, b. 80% power deposition, c, 60% power deposition and d. 50% power deposition. The corresponding absolute maximum global heat addition values are $q_{max} = 158.87$ at $s = 18.8$, 167.31 at $s = 23.2$, 181.66 at $s = 33.6$ and 157.94 at 46.8, respectively.
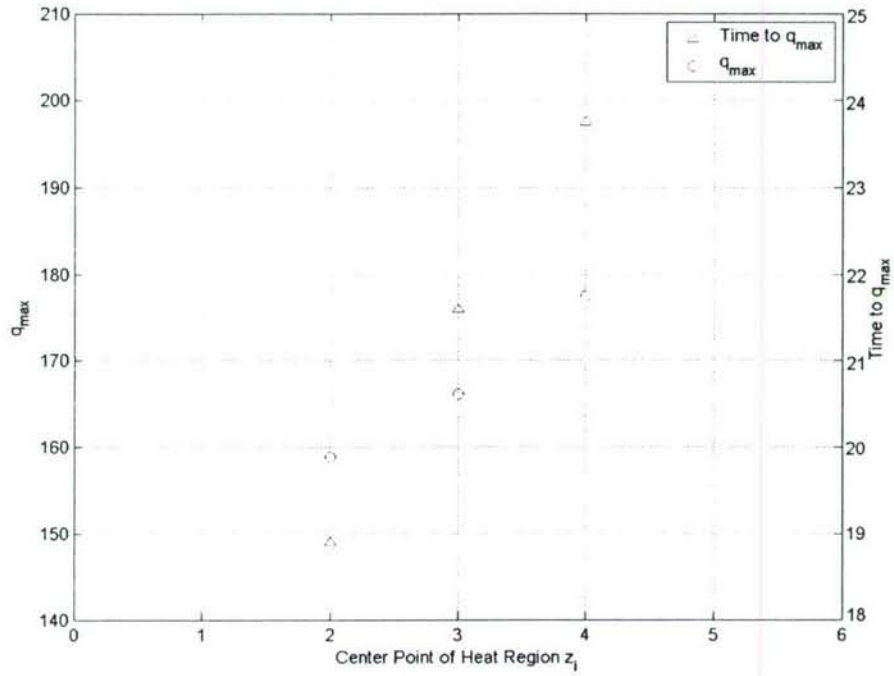
Figure 19. The variation of the absolute maximum global heat release, q_{max}, and the time to q_{max} with z_i for 100% power deposition when $\varepsilon^* = 0.0725$.
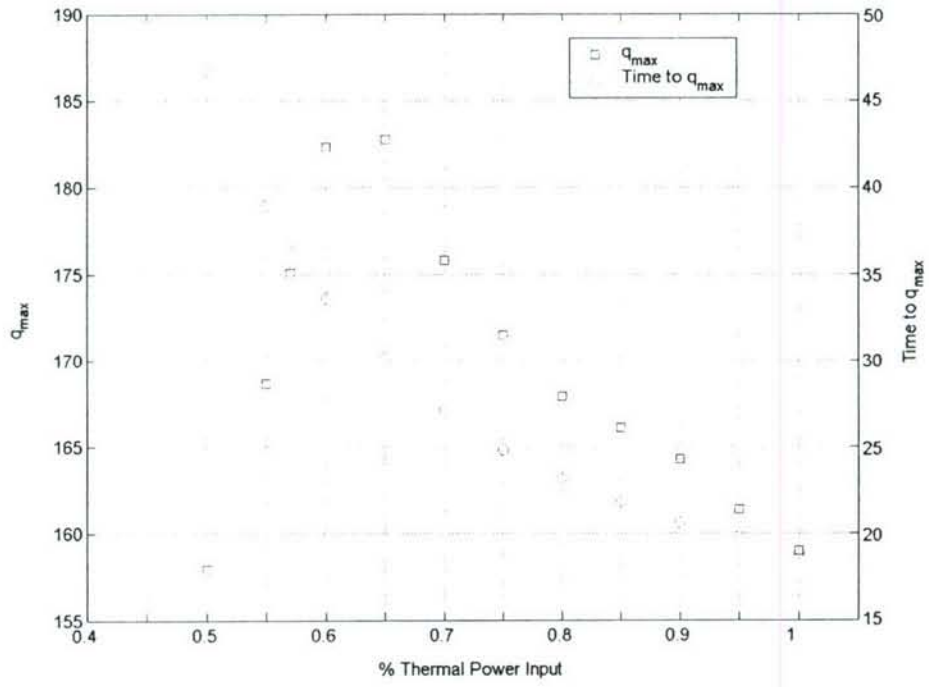
Figure 20. The variation of the absolute maximum global heat release, q_{max}, and the time to q_{max} as a function of the % of initial power deposition, when $z_i = 2$ and $\varepsilon^* = 0.0725$.

Figure 21. The time dependence of the instantaneous global maximum pressure, p_{max}, corresponding to the appearance of an overdriven detonation and subsequent relaxation to the C.J. value for a steady detonation wave when $z_i = 2$ and $\varepsilon^* = 0.0725$: a. 100% power deposition, b. 80% power deposition, c. 60% power deposition and d. 50% power deposition. The corresponding maximum pressures are 38.77 at $s = 20.8$, 40.74 at $s = 24.8$, 46.91 at $s = 34.6$, and 58.48 at $s = 46.4$.
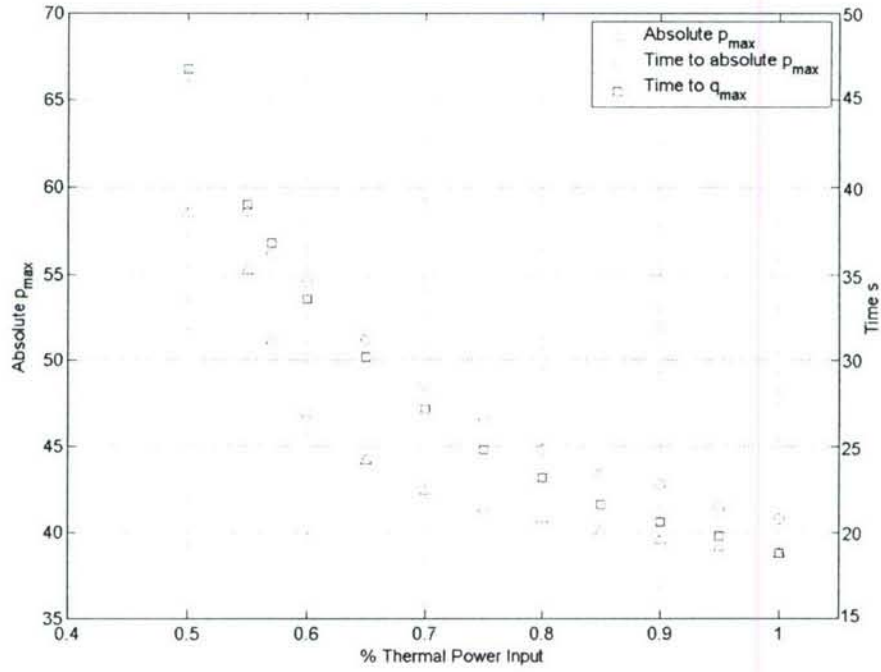
Figure 22. The variation of the absolute pressure maximum, $p_{max(abs)}$, and the time to $p_{max(abs)}$ for a range of initial power deposition levels when $z_i = 2$ and $\varepsilon^* = 0.0725$.
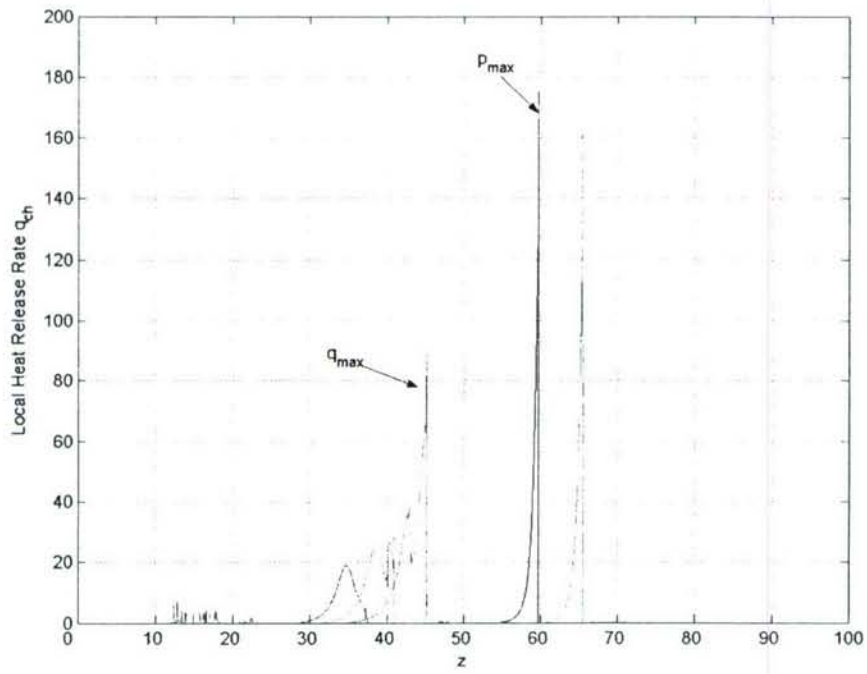
Figure 23. The time history of the local chemical heat release distributions with z, defined in Eq. 25, for the time values s = 16.8, 17.8, 18.8, 19.8, 21.4, 22.4 and 23.4 when $z_i = 2$ and $\varepsilon^* = 0.0725$.
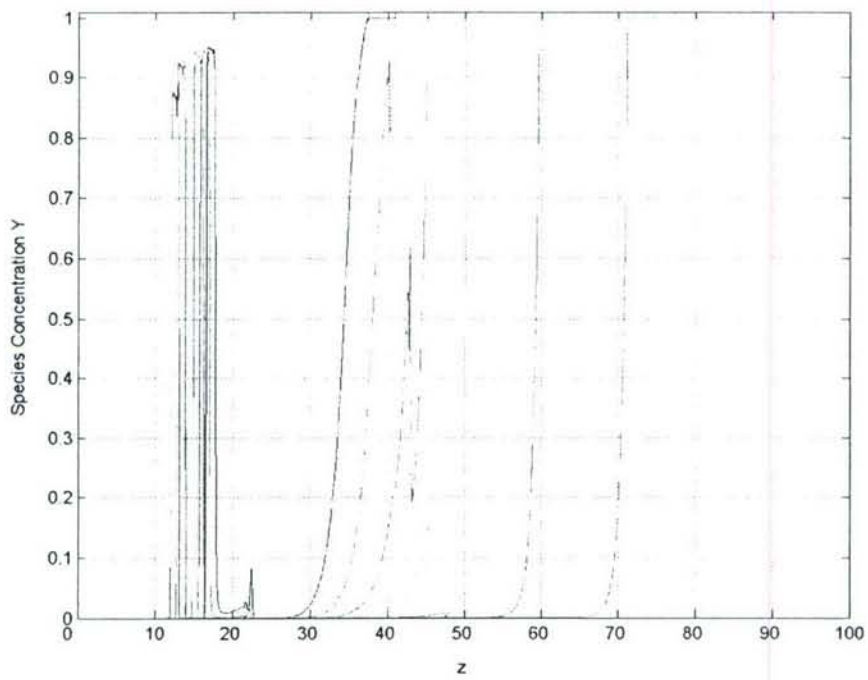
Figure 24. The time history of the species distributions with z for the time values s = 16.8, 17.8, 18.8, 19.8, 21.4, 22.4 and 23.4 when $z_i = 2$ and $\varepsilon^* = 0.0725$.
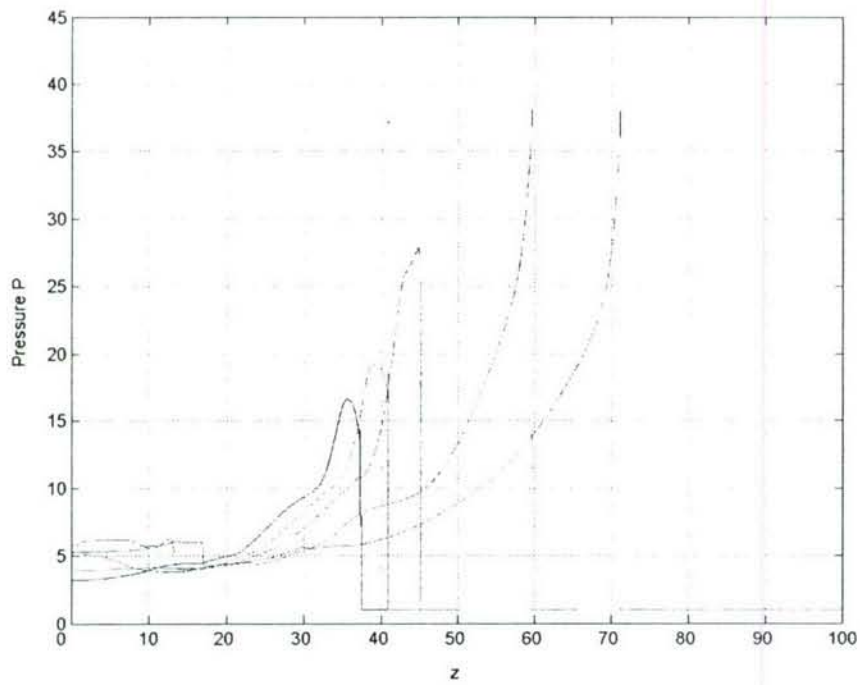
Figure 25. The time history of the pressure distributions with z for
the time values s = 16.8, 17.8, 18.8, 19.8, 21.4, 22.4 and 23.4 when
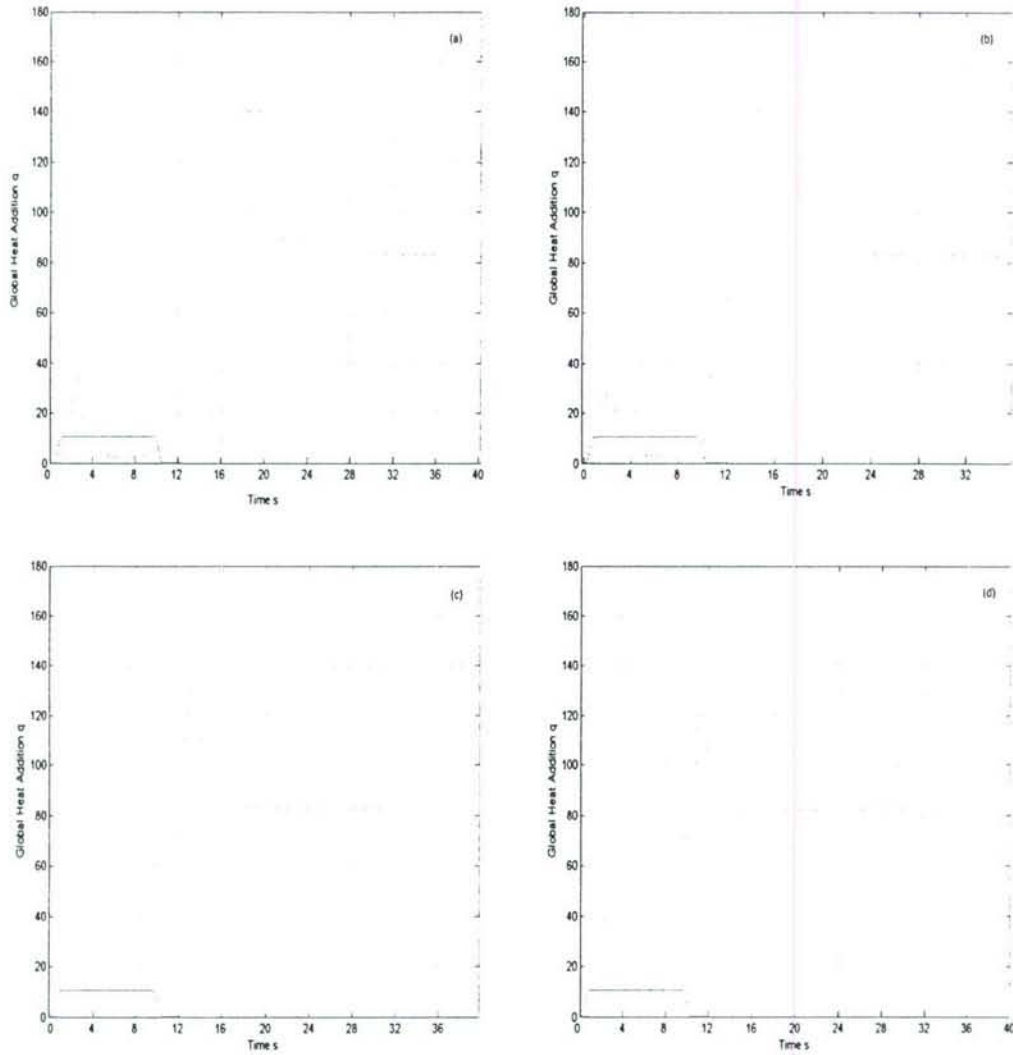$z_i = 2$ and $\varepsilon^* = 0.0725$.

Figure 26. The dependence of the global heat release, q, with time, s, on the activation energy parameter ε^*: a. $\varepsilon^*=0.0725$, $\varepsilon^*=0.0750$, $\varepsilon^*=0.0775$ and $\varepsilon^*=0.080$ when $z_i = 2$. The fourth local maximum is absorbed into the right side of the peak associated with the absolute maximum for the larger parameter values. The corresponding global heat addition maxima are; a. q_{max} = 158.9 at s = 18.8, b. q_{max} = 142.0 at s = 15.4, c. q_{max} = 130.6 at s = 13.2, and d. q_{max} = 124.0 at s = 11.4.
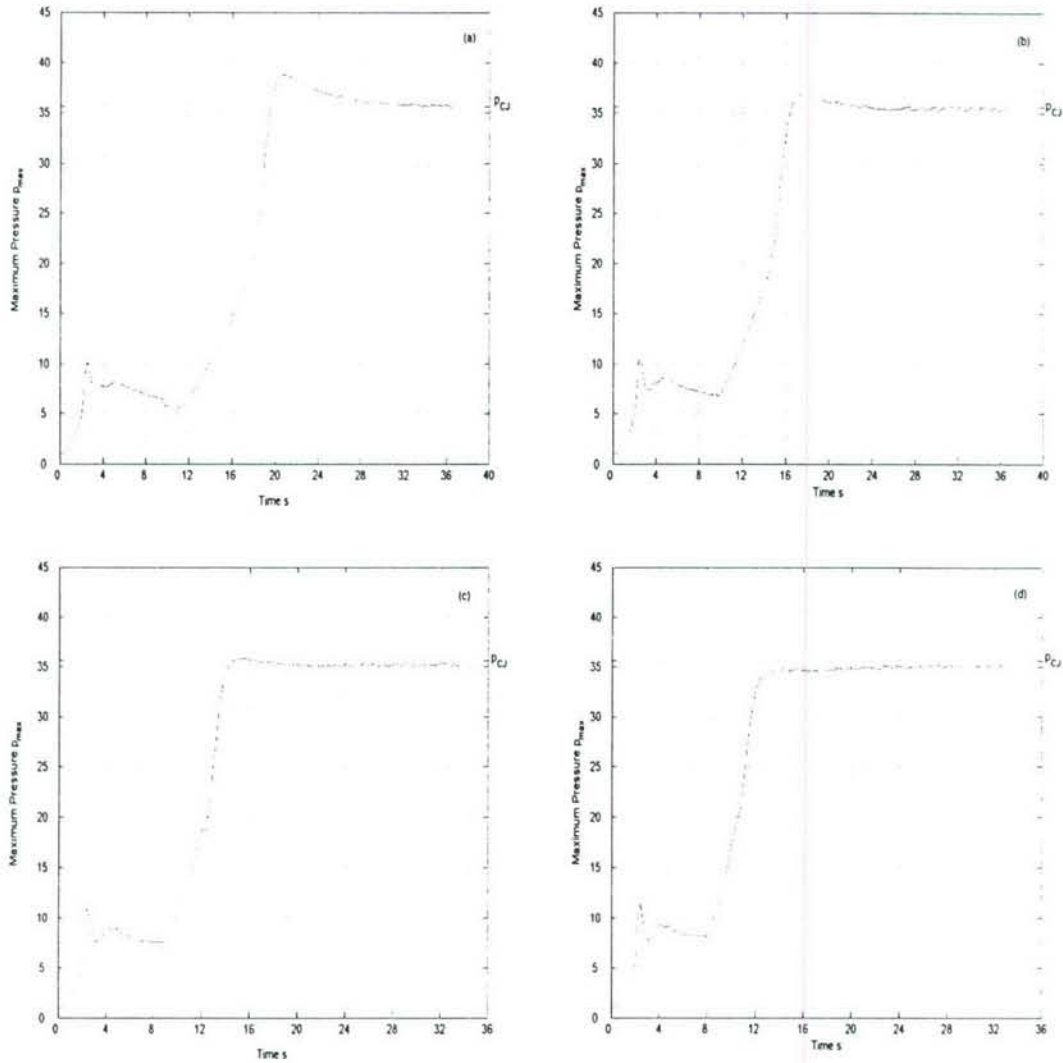
Figure 27. The time dependence of the instantaneous global maximum pressure, p_{max}, as a function of the activation energy values in Fig. 26, when $z_i = 2$ with 100% power deposition. When $\varepsilon^* = 0.080$ the pmax variation with time differs from that found for smaller values of ε^*. The corresponding absolute maximum pressure are 38.77 at $s = 20.8$, 36.99 at $s = 17.4$, 35.9668 at $s = 15.2$, and 35.29 at $s = 32.0$.
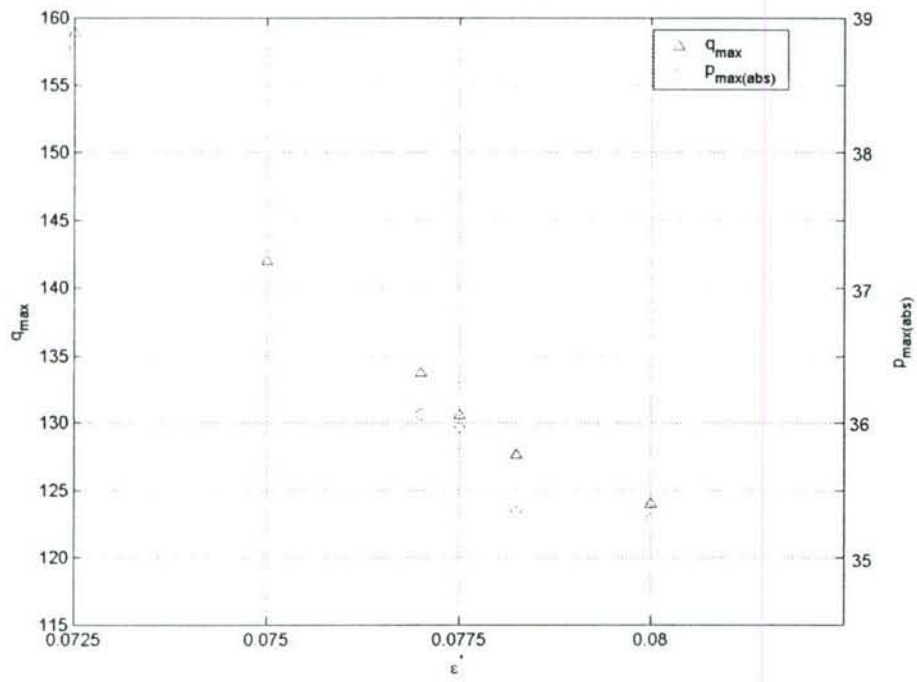
Figure 28. The variation of q_{max} (left scale) and $p_{max(abs)}$ (right scale) with activation energy parameter values, ε^*, for $z_i = 2$. Both quantities are sensitive to small variations in ε^*.
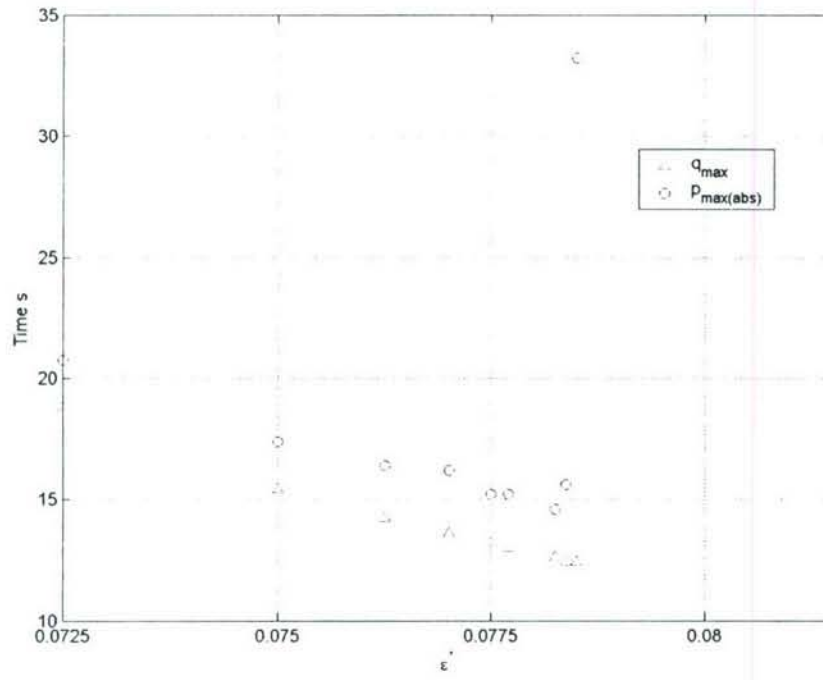
Figure 29. The dependence of the time to q_{max} and $p_{max(abs)}$ on the activation energy parameter value, ε^* for $z_i = 2$. The former shows a nearly linear monotonic decline with increasing values of ε^*, while the latter has an absolute maximum near $\varepsilon^* = 0.0775$.

Recent Publications Supported by AFOSR Grants

In addition to detonation initiation modeling, D.R.K and students continued to publish papers on solid rocket motor stability, based on work supported by an earlier AFOSR grant- Combustion Coupled Flow Dynamics in Solid Rocket Motors F49620-1-0175. These papers are denoted with an *

"Detonation Initiation and Evolution in a Model of a Pulsed Detonation Engine", with S. Palaniswamy, AIAA 2002-0612, 40th Aerospace Sciences Meeting, Reno, NV 2002

*"Acoustically Generated Unsteady Vorticity Field in a Long Narrow Cylinder with Sidewall Injection", with K. Kirkkopru, Q. Zhao and P.L. Staab, *J. Eng. Math.*, 42, 65-90, 2002

*"Three Dimensional Acoustic-Rotational Flows in a Cylinder with Sidewall Mass Addition", with P.L. Staab, *Physics of Fluids,* 14, #9, 3141-3159, 2002

"Modeling Detonation Initiation and Evolution in a Pulse Detonation Engine", with S. Palaniswamy,. AIAA 2003-1172, 41st Aerospace Sciences Meeting, Reno, NV. 2003

*"Acoustic-Rotational Internal Flow Caused by Transient Sidewall Mass Addition", with M.J. Rempe and P. L. Staab, *SIAM J. Applied Math.* **65,** #2, 587-617, 2005

"Modeling Detonation Initiation on the Microsecond Time Scale", with J.A. Kuehn, M.W. Nabity and J.F. Clarke, AIAA 2005-1169, 43rd Aerospace Sciences Meeting, Reno NV. 2005

"Detonation Initiation on the Microsecond Time Scale: Comparative Modeling", with J.A. Kuehn, M.W. Nabity and J.F. Clarke, AIAA-2006-0956, 44th Aerospace Sciences Meeting, Reno, NV. 2006

*"Internal Flow Temperature Dynamics in a Channel with Time-dependent Mass Injection", with A.M. Hegab, *AIAA J.*, **44,** #4, 812-826, 2007.

Detonation Initiation on the Microsecond Time Scale: DDT's, with J.A. Kuehn, M.W. Nabity and J.F. Clarke, submitted to Combustion Theory and Modeling, December, 2006

Detonation Initiation on the Microsecond Time Scale: One and Two Dimensional Results Obtained from Adaptive Wavelet-Collocation Numerical Methods, with J. Regele and O.V. Vasilyev, AIAA 2006-0986, 45th Aerospace Sciences Meeting, Reno, NV 2007

Project Personnel

i.   **D.R. Kassoy** is a Professor of Mechanical Engineering at the University of Colorado. He is the author of more than 100 technical publications in major journals for combustion, fluid dynamics and applied mathematics. His recent research has focused on solid rocket motor flow dynamics, detonation wave initiation and evolution in pulsed detonation engines and inertially confined thermal power deposition into gases.

ii.   **Keith Wojciechowski** has been a graduate student in the Department of Applied Mathematics in the University of Colorado. He recently left the program to pursue his PhD. Degree in Mathematics at another institution.

iii. **Matt Nabity** has been a graduate student in the Department of Applied Mathematics. He recently left the program to pursue his PhD. Degree in Mathematics at another institution.

iv. **Seth Friedly** was a graduate student in the Department of Mechanical Engineering. He received his M.S. degree in May 2004 and is currently employed in industry.

v.   **Jeff Lefcourt** was an undergraduate in the Department of Applied Mathematics. He received his degree in May 2004.

Presentations

- D. R. Kassoy, "Fireballs: Very Rapid Detonation Initiation by Transient, Spatially Resolved Thermal Power Deposition", International Colloquium on Dynamics of Explosions and Reactive Systems, Hakone, Japan, July 2003
- Seth Friedly and D.R. Kassoy, "A Model for the Evaporation of LOX Droplets in Cryogenic Hydrogen Gas". Graduate Seminar Series, Department of Mechanical Engineering, University of Colorado, Boulder, October 2003
- D.R. Kassoy, "Fireballs-Very Rapid Detonation Initiation by Transient, Spatially Resolved Thermal Power Deposition", Mechanical and Aerospace Engineering Department, Rutgers University, November 2003
- D. R. Kassoy, "Fireballs: Detonation Initiation on the Micro-second Time Scale", Annual Meeting of the Division of Fluid Dynamics of the American Physical Society, The Meadowlands, New Jersey, November 2003
- D.R. Kassoy, Vorticity and Heat Transfer Transients in a Model of a Solid Rocket Motor Chamber, CNES Toulouse, France, and ONERA, Toulouse, France, October 2004.
- D.R. Kassoy, Detonation Initiation by Thermal Power Deposition, 57th Division of Fluid Dynamics Meeting of the American Physical Society, Seattle, WA. November, 2004.
- D.R. Kassoy, Evaporation of a LOX Droplet in a Cold Hydrogen Gas, University of East Anglia, Norwich, England, Dec. 2004
- D.R. Kassoy, J.A. Kuehn, M.W. Nabity and Clarke, J.F., Modeling Detonations on the Microsecond Timescale, AIAA 2005-1169, 43rd Aerospace Sciences Meeting and Exhibit, Reno, NV, Jan. 2005
- D.R. Kassoy and M.W. Nabity, New Perspectives on Detonation Initiation: Fireball Formation on the Microsecond Timescale, Western States Section of the Combustion Institute, Standford University, October, 2005.
- D.R. Kassoy and M.W. Nabity, Detonation Initiation on the Microsecond Timescale: DDT's, Division of Fluid Dynamics Meeting of the American Physical Society, Chicago, IL, November 2005.
- D.R. Kassoy, J.A. Kuehn, M.W. Nabity and Clarke, J.F.,, Detonation Initiation on the Microsecond Timescale: Comparative Modeling, AIAA-

2006-0965, 44th Aerospace Sciences Meeting and Exhibit, Reno NV. January 2006

- D.R. Kassoy, Compressible fluid response to extremely rapid thermal power deposition, Division of Fluid Dynamics Meeting of the American Physical Society, Tampa FL. Nov 2006
- D.R. Kassoy, J.D. Regele, O.V. Vasilyev, Detonation Initiation on the Microsecond Timescale: Comparative One and Two Dimensional DDT Results from Adaptive Wavelet-Collocation Numerical Methods, 45th Aerospace Sciences Meeting and Exhibit, Reno NV. Jan 2007.
- D.R. Kassoy, Detonation Initiation on the Microsecond Timescale, Mechanical Engineering Department, University of Colorado, February 2007.
- D.R. Kassoy, Confessions of a Master Perturbator: A Matter of Scales, Applied Mathematics Colloquium, University of Colorado, February, 2007.